

# ELECTRONIC STRUCTURE STUDIES ON NMR SPIN-SPIN COUPLING AND NUCLEAR SHIELDING TENSORS

PERTTU LANTTO

*Department of Physical Sciences  
University of Oulu  
Finland*

Academic Dissertation to be presented with the assent of the Faculty of Science,  
University of Oulu, for public discussion in the Auditorium L10 (Raahensali), on  
November 30<sup>th</sup>, 2002, at 12 o'clock noon.

OULU 2002 • UNIVERSITY OF OULU

**Lantto, Perttu: Electronic structure studies on NMR spin-spin coupling and nuclear shielding tensors**

Department of Physical Sciences, University of Oulu, P.O.Box 3000, FIN-90014 University of Oulu, Finland

*Report Series in Physical Sciences No. 24 (2002)*

**Abstract**

In the present thesis the static tensor parameters of NMR spectroscopy are treated theoretically from first principles. The experimental NMR spin Hamiltonian and the observable spectral parameters in both isotropic (gases and ordinary liquids) and anisotropic environments (uniaxial liquid crystals) are presented. The non-relativistic and leading relativistic terms in the theory of nuclear spin-spin coupling  $\mathbf{J}$  and nuclear magnetic shielding  $\sigma$ , are discussed.

The conditions for accurate computational determination of the NMR parameters are investigated. The selection of one-electron basis sets as well as electron correlation are studied in detail by using *ab initio* multiconfigurational self-consistent field (MCSCF) theory. Reliable  $\mathbf{J}$  tensors are obtained only with large molecular orbital active spaces to include enough dynamical and static correlation. Core-valence correlation effects arising from semicore orbitals are necessary to include in couplings involving second-row elements.

The anisotropic indirect contribution to experimental anisotropic couplings was found to be negligible in  $^{13}\text{C}-^{13}\text{C}$ , as well as  $^{19}\text{F}-^{19}\text{F}$ , and  $^{13}\text{C}-^{19}\text{F}$  couplings (the latter two in non-aromatic systems), enabling experimental structure and/or orientation determination in anisotropic phases. For  $^{13}\text{C}-^{29}\text{Si}$  coupling and  $^{19}\text{F}$  couplings in aromatic systems, this may not hold.

The ability of the current generation of density-functional theory (DFT), particularly that of the hybrid B3LYP functional, to produce reliable anisotropic properties of  $\mathbf{J}$  tensors is found to be reasonable for first- and second-row elements other than halogens.

The relativistic spin-orbit (SO) effects on the rovibrational corrections to carbon nuclear shielding at finite temperature are found to be significant for a series of molecules containing heavy main group nuclei. In particular, the SO coupling is found to fully resolve the discrepancy of experimental secondary isotope effects and non-relativistic theory.

**Keywords:** NMR spectroscopy, spin Hamiltonian, spin-spin coupling, nuclear shielding, first principles, *ab initio*, electronic structure calculation, rovibrational effects, relativistic spin-orbit effects

## Acknowledgements

The work of the present thesis and my graduate studies took place in the NMR Research Group at the Department of Physical Sciences, University of Oulu, Finland. I would like to thank the former head of of the Department of Physical Sciences, Professor Emeritus Rauno Anttila and his successor Professor Jukka Jokisaari for placing the facilities at my disposal.

It has been my privilege to be supervised by Docent Juha Vaara, who has taught me the critical scientific approach to explain the mysteries of nature. I admire his knowledge of fundamental physics as well as his unfailing ability to compose interesting research subjects concerning wide range of physics from the fundamental theoretical level to the fruitful cooperation with experimental researchers. During the course of this work we have also become good friends and the many discussions concerning other subjects than science have been a good counterbalance to work.

The members of the NMR Research Group, past and present, are thanked for the great working atmosphere where the cooperation and friendship have been formed naturally. Also the rest of the academic, technical, and secretarial people of our department deserve many thanks for pleasant and friendly working environment.

In addition to Professor Jukka Jokisaari and Docent Juha Vaara, I have had the privilege to work with doctoral students Ville-Veikko Telkki, Anu Kantola, and Jyrki Schroderus, Doctors Jaakko Kaski and Bernd Schimmelpfennig, and Professors Tapio Rantala, Kenneth Ruud, and Trygve Helgaker. I also want to acknowledge the following people for inspiring and educational discussions: Doctor Tommi Matila, Docent Juhani Lounila, and Professors Roderick E. Wasylishen and Martin Kaupp.

I would like to thank Professors Pekka Pyykkö and Gustavo Adolfo Aucar for reviewing and commenting the thesis.

I gratefully acknowledge the financial support of present work by the Finnish Cultural Foundation, the Alfred Kordelin Foundation, the Magnus Ehrnrooth Foundation, the Pohjois-Pohjanmaa Fund of Finnish Cultural Foundation, the Tauno Tönning Foundation, the Oskar Öflund Foundation, and the Vilho, Yrjö and Kalle Väisälä Foundation. The Center for Scientific Computing (CSC), Espoo, Finland, is thanked for computing facilities that have made this work possible.

I am greatly indebted to all my dear friends for making my life so rich and

enjoyable. You are the ones to thank for the many memorable moments. Although the truth is in physics, the life is out there...

I feel deep gratitude to my parents, Liisa and Martti, and my sister Irina, for their love and support. Thanks to the upbringing, I have always been interested in finding out the reasonable explanations for the phenomena of the world.

I want to express my deepest love for my fiancée, Anu, with whom I have the privilege to share my life. I am profoundly grateful for her love and encouragement.

Oulu, November 2002

Perttu Lantto

## List of original papers

The present thesis consists of an introductory part and the following six papers, which are referred to in the text by their Roman numerals:

- I Kaski J, Lantto P, Vaara J & Jokisaari J (1998) Experimental and theoretical *ab initio* study of the  $^{13}\text{C}$ – $^{13}\text{C}$  spin-spin coupling and  $^1\text{H}$  and  $^{13}\text{C}$  shielding tensors in ethane, ethene and ethyne. *Journal of the American Chemical Society* 120: 3993–4005.
- II Kaski J, Lantto P, Schroderus J, Rantala T, Vaara J & Jokisaari J (1999) Experimental and theoretical study of the spin-spin coupling tensors in methylsilane. *The Journal of Physical Chemistry A* 103: 9669–9677.
- III Lantto P, Kaski J, Vaara J & Jokisaari J (2000) Spin-spin coupling tensors in fluoromethanes. *Chemistry – A European Journal* 6: 1395–1406.
- IV Lantto P & Vaara J (2001) Effect of correlating core orbitals in calculations of nuclear spin-spin couplings. *The Journal of Chemical Physics* 114: 5482–5490.
- V Lantto P, Vaara J & Helgaker T (2002) Spin-spin coupling tensors by the density-functional linear response theory. *The Journal of Chemical Physics* 117: 5998–6009.
- VI Lantto P, Vaara J, Kantola A M, Telkki V-V, Schimmelpfennig B, Ruud K & Jokisaari J (2002) Relativistic spin-orbit coupling effects on secondary isotope shifts of  $^{13}\text{C}$  nuclear shielding in  $\text{CX}_2$  ( $X = \text{O}, \text{S}, \text{Se}, \text{Te}$ ). *Journal of the American Chemical Society* 124: 2762–2771.

The Papers I, II, III, and VI contain both theoretical *ab initio* calculations of NMR parameters of small molecules and their experimental investigations in different environments. The Papers IV and V are purely theoretical studies.

The author performed most of the calculations and took part in their analysis as well as in writing of the manuscript in Paper I. He also participated in the planning and analyzing of Papers II, III, IV, and VI performing all the quantum chemical calculations. The rovibrational calculations of Paper VI as well as planning, performing, and analyzing of all the calculations in Paper V have been the

responsibility of the author. The first versions of the corresponding chapters in the manuscripts of Papers II, III, IV, V, and VI were written by the author. All the manuscripts were finished as teamwork.

## Abbreviations

BLYP	exchange-correlation functional with LYP correlation and Becke exchange
B3LYP	hybrid three-parameter BLYP with exact exchange
BP	Breit-Pauli (Hamiltonian)
CAS	complete active space (method)
CC	coupled-cluster (theory)
CCSD	coupled-cluster with single and double excitations
CCSD(T)	CCSD with non-iterative triple excitations
CVC	core-valence correlation
DF	Dirac-Fock (method)
DFT	density-functional theory
DK	Douglas-Kroll (method)
DSO	diamagnetic spin-orbit (interaction)
EFG	electric field gradient
EOM	equation-of-motion (method)
FC	Fermi contact (interaction)
FCI	full configuration interaction
FW	Foldy-Wouthuysen (transformation)
GIAO	gauge-including atomic orbital
HF	Hartree-Fock (theory)
IGLO	individual gauges for localized orbitals (method)
LC	liquid crystal
LDA	local density approximation
LORG	localized orbital/local origin (method)
LR	linear response (method)
MCSCF	multiconfigurational self-consistent field (theory)
MP2	second-order Møller-Plesset perturbation theory

NMR	nuclear magnetic resonance
NON	natural occupation numbers
NR	non-relativistic
PAS	principal axis system
PSO	paramagnetic spin-orbit (interaction)
QED	quantum electrodynamics
RAS	restricted active space (method)
RHF	restricted Hartree-Fock
SCF	self-consistent field
SD	spin-dipole (interaction)
SD/FC	spin-dipole/Fermi contact cross-term
SIC	self-interaction correction
SO	spin-orbit (coupling)
SOPPA	second-order polarization propagator approach
SR	scalar relativistic
ZORA	zeroth-order regular approximation

# Contents

Abstract	
Acknowledgements	
List of original papers	
Abbreviations	
Contents	
1 Introduction . . . . .	11
1.1 Outline of the thesis . . . . .	12
2 NMR spectral parameters . . . . .	14
2.1 Spin Hamiltonian . . . . .	14
2.2 Symmetry and tensorial properties . . . . .	16
2.2.1 Principal axis system . . . . .	17
2.2.2 Spin-spin coupling tensor $\mathbf{J}$ . . . . .	18
2.2.3 Nuclear shielding tensor $\sigma$ . . . . .	19
3 Electronic Hamiltonian . . . . .	21
3.1 Dirac equation . . . . .	21
3.2 Breit-Pauli Hamiltonian . . . . .	22
3.3 Contributions to NMR parameters . . . . .	24
3.3.1 Contributions to spin-spin coupling . . . . .	27
3.3.2 Contributions to shielding . . . . .	31
4 Computation of spin-spin coupling . . . . .	35
4.1 Summary of the papers . . . . .	35
4.2 One-electron basis set . . . . .	36
4.3 Many-electron effects . . . . .	38
4.3.1 Electron correlation . . . . .	38
4.3.2 Static and dynamical correlation effects in $\mathbf{J}$ . . . . .	39
4.3.3 Core-valence correlation . . . . .	41
4.4 Tensorial properties . . . . .	42
4.4.1 <i>Ab initio</i> calculations . . . . .	42
4.4.2 Density-functional theory calculations . . . . .	45
5 Computation of shielding . . . . .	52
5.1 One- and many-electron description . . . . .	52
5.2 Spin-orbit corrections to carbon shielding . . . . .	53

5.3	Rovibrational corrections and isotope effects . . . . .	54
5.3.1	Isotope shifts of $^{13}\text{C}$ shielding constants . . . . .	55
6	Conclusions . . . . .	58
	References . . . . .	61
	Original papers . . . . .	66

# 1 Introduction

In nuclear magnetic resonance (NMR) spectroscopy [1, 2], the interaction between the magnetic field and the intrinsic quantum mechanical angular momentum of the nucleus, the nuclear spin, is explored. Transitions between the quantized Zeeman energy levels of the nucleus in the magnetic field are observed as resonance peaks in the NMR spectrum. In molecules, small changes in the energies of the Zeeman states, caused by the magnetic field from other nearby nuclei as well as the interaction with the surrounding electrons, give rise to complicated fine structure in the spectra. The parameters describing these changes are the subject of this thesis. They convey information about the atomic and electronic structure of the molecule, the effects of rotation and vibration, as well as the interactions with the surrounding environment. This diversity of information and the ability to use the NMR method in all states of matter, gas, liquid (including also the more exotic liquid crystal (LC) environment), and solid, are reasons for placing NMR spectroscopy among the most influential experimental methods in the atomic and molecular studies in a variety of scientific disciplines: physics, chemistry, biosciences, materials science, and medicine. As the NMR parameters are determined by the hyperfine interactions between nuclei and electrons, they also provide an interesting object for theoretical quantum mechanical studies using first principles methods of electronic structure calculation.

The calculation of NMR parameters has lately become increasingly feasible due to development of theoretical methods and great advances in computer technology. Accounting for special relativity, as well as the effects arising from thermal motion, and interactions with the environment, are currently under intense investigation. The correlated *ab initio* wave function methods [3] having a character to systematically converge on both one- and many electron levels, provide exploration of these effects with unbiased fashion. On the other hand, density-functional theory (DFT) [4], where mostly semi-empirically parametrized exchange-correlation functionals are used to incorporate many-electron effects, has attracted tremendous theoretical interest and has been developed into a pragmatical tool for solving real chemical and materials science problems.

In both computational and experimental branches of NMR research, an increasing amount of so-called black-box methods are used. On the experimental side this

means that highly sophisticated, easy-to-use, spectrometers are used. Basic knowledge of the NMR theory is not a precondition for using NMR in applied research, as even the spectral analysis can be carried out by the spectrometer software. Also in computational chemistry, “black-box” codes provide a tool for carrying out highly complex calculations without hardly any theoretical background. The risk of course is that the consequences of the approximations used may not be understood. Therefore, thorough theoretical investigations of the different factors affecting NMR parameters are important in order to ensure that the applied methods stand on firm foundation.

## 1.1 Outline of the thesis

In the present thesis, we study the demands of tensorial NMR parameters on the level of theoretical description in first principles electronic structure calculations. Particularly, the correlation treatment in the case of spin-spin coupling tensor  $\mathbf{J}$  [5], is focussed upon. In addition, the rovibrational and relativistic effects on the NMR nuclear shielding tensor  $\sigma$  [6, 7], are investigated. The tensorial properties of  $\mathbf{J}$  and  $\sigma$  are of special interest since a significant part of the present thesis (Papers I–III and VI) was carried out in collaboration with the experimental NMR group at the University of Oulu. The group concentrates on the study of anisotropic materials using mainly atoms or small molecules as guests in either uniaxial LC or zeolite environments [8, 9, 10] where the tensorial properties and not merely their isotropic averages, are affecting the spectra.

In Papers I–III, the anisotropic parts of  $\mathbf{J}$  tensors involving  $^{13}\text{C}$ ,  $^{19}\text{F}$ , and  $^{29}\text{Si}$  nuclei, are investigated to obtain reliable estimates of their contribution to the experimentally observable anisotropic couplings. The latter are commonly used in the determination of the orientational and/or structural parameters of molecules in LC environments, for example in the structure determination of weakly oriented biomacromolecules [11]. The goal is to produce, independent of the experiment, information, which can either be used to aid in the analysis of experimental data or provide reliable data for comparison. Paper IV concentrates on the characteristics of the many-electron description necessary for accurate calculations of  $\mathbf{J}$  and  $\sigma$  in systems containing elements from the first and second rows of the periodic table. In these four studies, the *ab initio* multiconfigurational self-consistent field method (MCSCF) [3] using a linear response (LR) method for the calculation of properties (MCSCF LR) has been used. The computationally efficient DFT linear response (DFT LR) method, with various exchange-correlation functionals including for the first time also the hybrid B3LYP functional, is tested for  $\mathbf{J}$  in Paper V. The relativistic spin-orbit (SO) effect on the averaging over vibrational and rotational motion at finite temperatures, is studied in Paper VI for  $^{13}\text{C}$  shielding in systems containing heavy elements. Rovibrational averaging makes it possible to investigate also the secondary isotope shifts, *i.e.* shielding changes arising from different isotopic substitutions of the neighboring nuclei, together with their temperature effects.

The main part of the work presented in this thesis is contained in the Papers I–VI. The purpose of the following chapters is to introduce the basic concepts necessary for understanding the details of the papers. In Chapter 2, the basic theory of NMR parameters appearing in the NMR spin Hamiltonian is introduced, and the contributions to the spectra taken from isotropic (gas or liquid) or anisotropic (uniaxial LC) samples are examined. The electronic theory of the NMR parameters, starting from the relativistic Dirac Hamiltonian, is described in Chapter 3, leading to presentation of the terms contributing to spin-spin coupling and nuclear shielding tensors. In Chapters 4 and 5, the computational requirements posed by  $\mathbf{J}$  and  $\sigma$  are treated in more detail, concentrating on the one- and many-electron description at both MCSCF and DFT levels of theory. Chapter 5 is concerned with the effect of SO coupling on the rovibrational averaging effects on  $\sigma$ . The summary of the present thesis is given in Chapter 6.

## 2 NMR spectral parameters

In NMR spectroscopy, the external magnetic field causes energy differences between the spin states of the nuclei. Transitions between the states can be induced using radio-frequency excitation pulses. Upon returning to its thermal equilibrium, the spin system transmits a radio-frequency signal from which the NMR spectrum is obtained by Fourier transformation. The spectrum is interpreted in terms of an effective NMR spin Hamiltonian,  $H_{\text{NMR}}$ , where only the interaction of the nuclear spin  $\mathbf{I}_K$  with the external magnetic field  $\mathbf{B}_0$ , as well as other nuclear spins  $\mathbf{I}_L$  occur. The interaction parameters are obtained by fitting the energy eigenvalue spectrum of  $H_{\text{NMR}}$  to the experimental spectrum. The NMR spectral parameters are introduced in the following section.

### 2.1 Spin Hamiltonian

The dimensionless quantum mechanical electron spin  $\mathbf{s}_i$  is associated with the magnetic moment  $\boldsymbol{\mu}_i$  of a free electron  $i$  (in SI-units)<sup>1</sup>

$$\boldsymbol{\mu}_i = -\frac{e\hbar}{2m_e}g_e \mathbf{s}_i, \quad (2.1)$$

where  $g_e = 2.0023193043737\{82\}$  [12] is the free-electron  $g$ -factor and the other symbols have their usual meanings. Similarly, the nuclear magnetic moment is a consequence of the dimensionless nuclear spin  $\mathbf{I}_K$

$$\boldsymbol{\mu}_K = \gamma_K \hbar \mathbf{I}_K, \quad (2.2)$$

where  $\gamma_K$  is the gyromagnetic ratio of the nucleus. The interaction energy of  $\boldsymbol{\mu}_K$  with an external magnetic field is quantized to the  $(2I + 1)$  values with  $m_I = -I, -I + 1, \dots, I - 1, I$ :

$$E = -\boldsymbol{\mu}_K \cdot \mathbf{B}_0 = -\gamma_K \hbar m_I B_0. \quad (2.3)$$

---

<sup>1</sup>SI-units are consistently used in this thesis, unless otherwise noted.

In the case of a static and homogeneous external magnetic field, the Hamiltonian that describes static interactions in the NMR spectrum can be written as a perturbation expansion of the ground state energy around  $\mathbf{B}_0 = \boldsymbol{\mu}_K = \boldsymbol{\mu}_L = \mathbf{0}$ , with  $\mathbf{B}_0$ ,  $\boldsymbol{\mu}_K$ , and  $\boldsymbol{\mu}_L$  treated as small perturbations

$$\begin{aligned} E &= E_0 + \mathbf{E}_{\mathbf{B}_0} \cdot \mathbf{B}_0 + \sum_K \mathbf{E}_{\boldsymbol{\mu}_K} \cdot \boldsymbol{\mu}_K \\ &+ \frac{1}{2} \mathbf{B}_0 \cdot \mathbf{E}_{\mathbf{B}_0, \mathbf{B}_0} \cdot \mathbf{B}_0 + \sum_K \boldsymbol{\mu}_K \cdot \mathbf{E}_{\boldsymbol{\mu}_K, \mathbf{B}_0} \cdot \mathbf{B}_0 \\ &+ \frac{1}{2} \sum_{KL} \boldsymbol{\mu}_K \cdot \mathbf{E}_{\boldsymbol{\mu}_K, \boldsymbol{\mu}_L} \cdot \boldsymbol{\mu}_L + \dots, \end{aligned} \quad (2.4)$$

where molecular properties correspond to the energy derivatives with respect to the static perturbations

$$\mathbf{E}_{\mathbf{a}} = \left. \frac{\partial E}{\partial \mathbf{a}} \right|_{\mathbf{a}=\mathbf{0}} \quad (2.5)$$

$$\mathbf{E}_{\mathbf{a}, \mathbf{b}} = \left. \frac{\partial^2 E}{\partial \mathbf{a} \partial \mathbf{b}} \right|_{\mathbf{a}=\mathbf{b}=\mathbf{0}}. \quad (2.6)$$

In closed-shell molecules, only the second- and higher-order derivatives remain for orbitally non-degenerate, singlet electronic ground-states, described by a real wave function. Higher than second-order terms are only rarely needed in NMR [13]. The spectrum is affected by the second-order derivatives, linear in either or both  $\boldsymbol{\mu}_K$  and  $\boldsymbol{\mu}_L$ , leading to the NMR spin Hamiltonian (in Hz)

$$\begin{aligned} H_{\text{NMR}} &= - \sum_K \frac{\gamma_K}{2\pi} \mathbf{I}_K \cdot (\mathbf{1} - \boldsymbol{\sigma}_K) \cdot \mathbf{B}_0 \\ &+ \sum_{K < L} \mathbf{I}_K \cdot (\mathbf{D}'_{KL} + \mathbf{J}_{KL}) \cdot \mathbf{I}_L, \end{aligned} \quad (2.7)$$

where  $\mathbf{1}$  is the unit tensor,  $\boldsymbol{\sigma}_K$  the nuclear magnetic shielding tensor of nucleus  $K$  and  $\mathbf{J}_{KL}$  is the indirect spin-spin coupling tensor between nuclei  $K$  and  $L$ . This expansion is valid for all  $\mathbf{I}_K$ . If  $I_K > \frac{1}{2}$ , further terms arise.

The direct dipole-dipole coupling tensor

$$\mathbf{D}'_{KL} = - \frac{\hbar}{2\pi} \frac{\mu_0}{4\pi} \gamma_K \gamma_L \left( \frac{3\mathbf{R}_{KL}\mathbf{R}_{KL} - \mathbf{1}R_{KL}^2}{R_{KL}^5} \right) \quad (2.8)$$

describes the direct interaction between the nuclear magnetic moments  $\boldsymbol{\mu}_K$  and  $\boldsymbol{\mu}_L$ .  $\mathbf{R}_{KL} = \mathbf{R}_K - \mathbf{R}_L$  is the relative position vector of the two nuclei.  $\mathbf{D}'_{KL}$  is cylindrically symmetric in the direction between coupled nuclei and can be used for the determination of structural and orientational parameters of the molecules.

For nuclei with  $I_K \geq 1$ , the interaction of the nuclear electric quadrupole moment with the electric field gradient at the nuclear site, affects the NMR spectrum. The corresponding spectral parameter is the nuclear quadrupole coupling tensor  $\chi_K$ .

The observable tensor components of all the previous interaction parameters are averages over the inter- and intramolecular motion, in the time scale of the NMR experiments, *i.e.*  $T = \langle T \rangle$ . The angular brackets denoting the time average are implicitly understood in the following.

## 2.2 Symmetry and tensorial properties

In isotropic surroundings, such as gases or ordinary liquids, all orientations of the molecule are equally probable. The rotation of the molecule is under normal circumstances fast enough to average the anisotropic interactions to zero in the time-scale of the NMR experiment. In that case, only the rank-0 isotropic average,  $T^{\text{iso}}\mathbf{1}$ , of the interaction tensor  $\mathbf{T}$  is left

$$T = T^{\text{iso}} = \frac{1}{3}\text{Tr } \mathbf{T}. \quad (2.9)$$

If the observed molecule is in an anisotropic environment, where the motion of the molecules is constrained, such as LCs, microporous materials like zeolites, the solid state, or it is adsorbed at a surface, only partial orientation and incomplete averaging of the tensorial observables result. This is observed in the NMR spectrum as increased complexity. As an example, in a uniaxial, anisotropic LC solution, the NMR spin Hamiltonian for spin- $\frac{1}{2}$  nuclei in the laboratory frame  $(x', y', z')$  becomes

$$\begin{aligned} H_{\text{NMR}}^{\text{LC}} &= -\frac{B_0}{2\pi} \sum_K \gamma_K (1 - \sigma_K - \sigma_K^{\text{aniso}}) I_{K,z'} \\ &+ \sum_{K < L} J_{KL} \mathbf{I}_K \cdot \mathbf{I}_L \\ &+ \sum_{K < L} \left( D_{KL} + \frac{1}{2} J_{KL}^{\text{aniso}} \right) (3I_{K,z'} I_{L,z'} - \mathbf{I}_K \cdot \mathbf{I}_L), \end{aligned} \quad (2.10)$$

where  $\mathbf{B}_0 = B_0 z'$ ,  $\sigma_K + \sigma_K^{\text{aniso}}$  is the nuclear magnetic shielding, where  $\sigma = \sigma_K^{\text{iso}}$  is the shielding constant and  $\sigma_K^{\text{aniso}}$  arises from the anisotropic part of shielding tensor.  $I_{K,z'}$  is the projection of the  $\mathbf{I}_K$  in the direction of the external magnetic field.  $J_{KL} = J_{KL}^{\text{iso}}$  is the spin-spin coupling constant and the anisotropic part of  $\mathbf{J}_{KL}$  gives rise to  $J_{KL}^{\text{aniso}}$  contribution. As  $\mathbf{D}'_{KL}$  is a traceless tensor, the direct dipole-dipole coupling  $D_{KL} = \frac{1}{2} D'_{KL}$  has no effect on the isotropic spectrum, which is therefore determined only by the  $\sigma_K$  and  $J_{KL}$ . In Eq. (2.10), the so-called high-field approximation is used, meaning that the direct Zeeman interaction of the nuclear spin with the external magnetic field

$$H_Z = -\frac{B_0}{2\pi} \sum_K \gamma_K I_{K,z'}, \quad (2.11)$$

is assumed to be significantly larger than the other interactions involved, rendering first-order perturbation theory for the latter a good approximation.

In anisotropic LC samples, the traceless and symmetric orientation tensor of Saupe [14] in the molecule-fixed coordinates

$$S_{\epsilon\tau}^D = \langle s_{\epsilon\tau} \rangle = \frac{1}{2} \langle 3 \cos \theta_{\epsilon, \mathbf{n}} \cos \theta_{\tau, \mathbf{n}} - \delta_{\epsilon\tau} \rangle; \quad \epsilon, \tau \in (x, y, z), \quad (2.12)$$

is characteristic of the orientational distribution of the solute molecules around the optical axis, director  $\mathbf{n}$ , of the liquid crystal phase. The anisotropic contribution arising from the interaction tensor  $\mathbf{T}$  is then

$$\begin{aligned} T^{\text{aniso}} &= \frac{2}{3} P_2(\cos \varphi) \sum_{\epsilon\tau} S_{\epsilon\tau}^D T_{\epsilon\tau} \\ &= \frac{2}{3} P_2(\cos \varphi) \left[ \Delta T S_{zz}^D + \frac{1}{2} (T_{xx} - T_{yy}) (S_{xx}^D - S_{yy}^D) \right. \\ &\quad \left. + 2 T_{xy}^S S_{xy}^D + 2 T_{yz}^S S_{yz}^D + 2 T_{xz}^S S_{xz}^D \right], \end{aligned} \quad (2.13)$$

where the second-order Legendre polynomial,  $P_2(\cos \varphi) = \frac{1}{2} (3 \cos^2 \varphi - 1)$ , changes the reference from the liquid crystal director frame to the laboratory  $(x', y', z')$  frame, with  $\varphi$  denoting the angle between  $\mathbf{B}_0$  and  $\mathbf{n}$ . Here, the approximation  $\langle s_{\epsilon\tau} T_{\epsilon\tau} \rangle = S_{\epsilon\tau}^D \langle T_{\epsilon\tau} \rangle$  is used, although it is not fully satisfied due to the correlation between rotational and vibrational motion, known as the deformation of the molecule [15, 16, 17]. In Eq. (2.13), the anisotropy of  $\mathbf{T}$  with respect to the (molecule-fixed)  $z$  direction is defined as

$$\Delta T = T_{zz} - \frac{1}{2} (T_{xx} + T_{yy}). \quad (2.14)$$

The rank-2 symmetric part of the tensor is

$$T_{\epsilon\tau}^S = \frac{1}{2} (T_{\epsilon\tau} + T_{\tau\epsilon}) - T \delta_{\epsilon\tau}. \quad (2.15)$$

Many of the anisotropic terms can often be dropped out due to the symmetry of small solute molecules.

### 2.2.1 Principal axis system

In solid powder samples, the diagonal components of the NMR tensors, represented in their principal axis system (PAS), are observable [18]. However, the directions of the principal axis are generally unavailable from powder spectra. In theoretical calculations, the PAS is obtained by solving the eigenvectors and eigenvalues of the symmetric part of the interaction tensor,  $T\mathbf{1} + \mathbf{T}^S$ . Using the eigenvectors, it is possible to transform the principal components from a powder experiment to the molecule-fixed frame, which makes them comparable with the results from LC experiments. The transformation from the molecule-fixed frame to PAS is

generally not possible because not all tensor components are always available from LC NMR experiment. In favorable situations, the coordinate system in which theoretical calculation is carried out, can be aligned with the principal axes of a certain tensor based on knowledge of the local symmetry. In this case, the diagonal elements can immediately be identified as principal components.

### 2.2.2 Spin-spin coupling tensor $\mathbf{J}$

The spin-spin coupling tensor describes the magnetic interaction between nuclear spins through the electron system. The hyperfine interaction with nucleus  $K$  produces a spin polarization of electrons which is then transmitted through the electron system and detected by nucleus  $L$  through another hyperfine interaction.

The so-called reduced spin-spin coupling is independent of the gyromagnetic ratios of the coupled nuclei, and therefore describes the purely electronic contribution. It can be presented as the second derivative of the total energy of the system (2.4)

$$\mathbf{K}_{KL} = \left. \frac{\partial^2 E(\boldsymbol{\mu}_K, \boldsymbol{\mu}_L)}{\partial \boldsymbol{\mu}_K \partial \boldsymbol{\mu}_L} \right|_{\boldsymbol{\mu}_K = \boldsymbol{\mu}_L = \mathbf{0}} - \hbar \mathbf{D}'_{KL}, \quad (2.16)$$

from which the total spin-spin coupling tensor of Eq. (2.7) is obtained as

$$\mathbf{J}_{KL} = \frac{1}{2\pi} \hbar \gamma_K \gamma_L \mathbf{K}_{KL}. \quad (2.17)$$

$\mathbf{J}_{KL}$  is a sum of rank-0, -1 and -2 tensors,

$$\mathbf{J}_{KL} = J_{KL} \mathbf{1} + \mathbf{J}_{KL}^A + \mathbf{J}_{KL}^S, \quad (2.18)$$

where the rank-0 contribution is the coupling constant  $J_{KL}$  according to Eq. (2.9), the rank-2 symmetric part  $\mathbf{J}_{KL}^S$  is defined in Eq. (2.15), and the rank-1 antisymmetric part is

$$J_{KL, \epsilon\tau}^A = \frac{1}{2} (J_{KL, \epsilon\tau} - J_{KL, \tau\epsilon}). \quad (2.19)$$

In a uniaxial LC environment, the anisotropic direct dipole-dipole coupling (2.8) appears in the spectrum together with the rank-2 anisotropic part of  $\mathbf{J}_{KL}$

$$D_{KL}^{\text{exp}} = D_{KL} + \frac{1}{2} J_{KL}^{\text{aniso}}, \quad (2.20)$$

as can be seen from Eqs. (2.10) and (2.13). Information on  $J_{KL}^{\text{aniso}}$  is obtainable also from LC experiments by subtracting from  $D_{KL}^{\text{exp}}$  the calculated  $D_{KL}$  (2.8) corrected for the effects of both harmonic [19] and anharmonic [20] molecular vibrations as well as the deformation effects caused by the correlation of vibrational and orientational motions [15, 16, 17]. The rank-1 antisymmetric contribution  $J_{KL}^A$  exists only if it generates the totally symmetric representation of the local point group of the coupling [21]. In strongly coupled systems it could have some effect on the relaxation rates, although this has not yet been observed experimentally [10].

The use of  $D_{KL}$  couplings is advantageous when examining very precise molecular structure or orientation in environment [8, 9, 10]. These studies provide information about interactions with solute molecules and fields. To reach high enough accuracy in the determination of  $D_{KL}$ , the  $J_{KL}^{\text{aniso}}$  contribution should potentially be taken into account in the analysis of experimental data. Whether this is necessary or not, is one of the main motivations of exploring the spin-spin coupling tensor with high accuracy, by theoretical first principles methods.

Being very sensitive for the details of the electronic structure, the spin-spin coupling tensor constitutes an interesting object for testing computational methods. To resolve the challenges set by  $\mathbf{J}_{KL}$ , both electronic structure theories as well as practical computational methods are under constant development [22].

### 2.2.3 Nuclear shielding tensor $\sigma$

The nuclear magnetic shielding tensor  $\sigma_K$  describes the magnetic field at the nucleus  $K$ , caused by the electric currents induced by the external magnetic field  $\mathbf{B}_0$ . These magnetic fields usually diminish the total field experienced by nucleus  $K$  *i.e.* they shield the nucleus. The components of the field of the nucleus can be written as

$$B_u^{\text{loc}} = \sum_v (\delta_{uv} - \sigma_{K,uv}) B_{0,v}; \quad u, v \in x, y, z \quad (2.21)$$

where  $u$  and  $v$  are the directions of the internal and external magnetic fields, respectively, in the molecule-fixed frame.  $\sigma$  contains generally nine independent components that can be divided into rank-0, -1, and -2 contributions [23], similarly to the case of  $\mathbf{J}$ . The symmetry of the molecule may decrease the number of independent components, however.

Shielding is always positive for a free atom, which means that the current-induced magnetic field acts in the opposite direction to the external field. Therefore, the local magnetic field  $\mathbf{B}^{\text{loc}}$  is weaker than the external magnetic field  $\mathbf{B}_0$ . In molecules, the more complex electronic structure caused by the presence of other nuclei, changes the currents and may occasionally lead also to negative shielding in which case the local field can be larger than the external one.

Nuclear magnetic shielding is a second-order property that can be defined as a second derivative from Eq. (2.7)

$$\sigma_K = \mathbf{1} + \left. \frac{\partial^2 E}{\partial \boldsymbol{\mu}_K \partial \mathbf{B}_0} \right|_{\mathbf{B}_0 = \boldsymbol{\mu}_K = \mathbf{0}}, \quad (2.22)$$

where the bare-nucleus Zeeman interaction (2.11) is eliminated by the unit tensor  $\mathbf{1}$ . Nuclear shielding is usually reported relative to the shielding of a similar nucleus located in a reference molecule. The quantity usually employed is the chemical shift

$$\delta_K = \frac{\nu_K - \nu_{K,\text{ref}}}{\nu_{K,\text{ref}}} = \frac{\sigma_{K,\text{ref}} - \sigma_K}{1 - \sigma_{K,\text{ref}}} \approx \sigma_{K,\text{ref}} - \sigma_K, \quad (2.23)$$

where the last form arises as the denominator is usually almost equal to one ( $1 - \sigma_{K,\text{ref}} \approx 1$ ). The chemical shift is therefore obtained by dividing the difference [ $\mathcal{O}(\text{Hz})$ ] of the resonance frequency  $\nu_K$  of the nucleus  $K$  in the studied molecule from the frequency  $\nu_{K,\text{ref}}$  of the same nucleus in the reference molecule, by  $\nu_{K,\text{ref}}$  [ $\mathcal{O}(10^6 \text{ Hz})$ ], unit becoming  $\text{ppm} = 10^{-6}$ . The chemical shift and nuclear shielding can be reported irrespective of the magnetic field strength.

## 3 Electronic Hamiltonian

Although the NMR parameters for light elements are well-treated by a Hamiltonian containing NR kinematics and Zeeman interactions, the need for relativistic treatment of NMR properties arises relatively early when going towards heavier elements in the periodic table. This is due to the fact that the NMR properties obtain large contributions from electrons residing close to the nuclei, where their velocities are high [24, 25]. The perturbational relativistic Hamiltonian for NMR calculations is presented in this chapter, followed by the introduction of both the NR and (briefly) the relativistic operators contributing to NMR parameters.

### 3.1 Dirac equation

The fundamental interactions between the electromagnetic field and electronic structure of matter are described by quantum electrodynamics (QED) [26, 27]. However, application of QED to the computation of NMR properties is very challenging and results have emerged only recently [28, 29]. Hence, the practical method is to start from the Dirac equation [26, 27, 30, 31, 32].

The time-independent Dirac equation for single electron in electromagnetic field is

$$H^D \Psi = E \Psi \quad (3.1)$$

$$H^D = c \boldsymbol{\alpha} \cdot \boldsymbol{\pi} + \beta m_e c^2 - e\phi \quad (3.2)$$

$$\boldsymbol{\pi} = -i\hbar\nabla + e\mathbf{A}, \quad (3.3)$$

where the momentum operator  $\boldsymbol{\pi}$  in Eq. (3.3) contains the vector potential  $\mathbf{A}$  of the electromagnetic field, and  $\phi$  in Eq. (3.2) is the potential.  $H^D$  contains the Dirac  $4 \times 4$  matrix operators  $\boldsymbol{\alpha}$

$$\alpha_\epsilon = \rho \otimes \sigma_\epsilon \quad \forall \epsilon \in (x, y, z); \quad \rho = \begin{pmatrix} \mathbf{0} & \mathbf{1} \\ \mathbf{1} & \mathbf{0} \end{pmatrix}; \quad \alpha_0 = \beta = \begin{pmatrix} \mathbf{1} & \mathbf{0} \\ \mathbf{0} & -\mathbf{1} \end{pmatrix}, \quad (3.4)$$

which are made up of the Pauli  $2 \times 2$  spin matrices

$$\sigma_x = \begin{pmatrix} 0 & 1 \\ 1 & 0 \end{pmatrix}; \quad \sigma_y = \begin{pmatrix} 0 & -i \\ i & 0 \end{pmatrix}; \quad \sigma_z = \begin{pmatrix} 1 & 0 \\ 0 & -1 \end{pmatrix}, \quad (3.5)$$

and act on the four-component wave function

$$\Psi = \begin{pmatrix} \psi_+ \\ \psi_- \end{pmatrix}; \quad \psi_+ = \begin{pmatrix} \psi_1 \\ \psi_2 \end{pmatrix}; \quad \psi_- = \begin{pmatrix} \psi_3 \\ \psi_4 \end{pmatrix}. \quad (3.6)$$

The wave function has also the so-called small-component  $\psi_-$ , which are small for electronic, positive energy solutions but large for positronic, negative energy solutions. This complicates the calculations and two-component approaches are welcome, where only the interesting electronic states,  $\psi_+$ , are treated.

### 3.2 Breit-Pauli Hamiltonian

The approximate relativistic many-electron Hamiltonian is constructed by assuming only pairwise additive interactions. Therefore, one can start from the so-called Dirac-Coulomb-Breit Hamiltonian [26, 27] for two electrons,  $i$  and  $j$ ,

$$H_{ij}^{\text{DCB}} = H_i^{\text{D}} + H_j^{\text{D}} + \frac{e_i e_j}{4\pi\epsilon_0 r_{ij}} \quad (3.7)$$

$$- \frac{e_i e_j}{8\pi\epsilon_0 r_{ij}} \left[ (\boldsymbol{\alpha}_i \cdot \boldsymbol{\alpha}_j) + \frac{(\boldsymbol{\alpha}_i \cdot \mathbf{r}_{ij})(\boldsymbol{\alpha}_j \cdot \mathbf{r}_{ij})}{r_{ij}^2} \right] \quad (3.8)$$

$$+ \mathcal{O}(m_e c^2 \alpha^5),$$

where the term (3.8), the Breit operator [33], corrects for the relativistically insufficient instantaneous Coulomb interaction to the order of  $\mathcal{O}(m_e c^2 \alpha^4)$ , where  $\alpha = e^2 \mu_0 c / 2h$  is the dimensionless fine structure constant. This Hamiltonian is still not completely Lorentz-invariant and the effects of QED are approximated using perturbation theory [26, 27]. It is only appropriate to use the first order of perturbation theory, for relatively small velocities.

A two-component Hamiltonian is obtained by decoupling the small and large components of four-component wave function (3.6). One way of doing this is to use the Foldy-Wouthuysen (FW) transformation [34], where  $H_{ij}^{\text{DCB}}$  (3.7–3.8) is transformed into two-component form by two unitary transformations [26, 27]. The coupling of positive and negative states, due to the  $c \boldsymbol{\alpha} \cdot \boldsymbol{\pi}$  operator, is eliminated to order  $\mathcal{O}(m_e c^2 \alpha^5)$ .

In order to obtain the molecular electronic Hamiltonian, also contributions from nuclei must be included. When using the Born-Oppenheimer approximation the nuclei are taken as an assembly of stationary charges and magnetic moments, leading to static nuclear electromagnetic fields. There are no terms in the Hamiltonian involving motion of the nuclei. Using  $(\boldsymbol{\alpha}_i \cdot \boldsymbol{\pi}_i)^2 = (\boldsymbol{\sigma}_i \cdot \boldsymbol{\pi}_i)^2$ ,

$\pi_i^2 + i\boldsymbol{\sigma}_i \cdot \boldsymbol{\pi}_i \times \boldsymbol{\pi}_i = \pi_i^2 + e\hbar\boldsymbol{\sigma}_i \cdot \mathbf{B}$ , and  $\boldsymbol{\sigma}_i = g_e\mathbf{s}_i$ , the final Breit-Pauli Hamiltonian can be written as

$$H_{ij}^{\text{BP}} = \sum_i h_i + \sum_{i<j} h_{ij}, \quad (3.9)$$

separated to one- ( $h_i$ ) and two-electron ( $h_{ij}$ ) parts, where (one-electron part)

$$h_i = -\frac{e^2}{4\pi\epsilon_0} \sum_K \frac{Z_K}{r_{iK}} \quad (3.10)$$

$$+ \frac{e^2\hbar^2}{8\epsilon_0 m_e^2 c^2} \sum_K Z_K \delta(\mathbf{r}_{iK}) \quad (3.11)$$

$$+ \frac{\pi_i^2 + e\hbar g_e \mathbf{s}_i \cdot \mathbf{B}}{2m_e} \quad (3.12)$$

$$- \frac{(\pi_i^2 + e\hbar g_e \mathbf{s}_i \cdot \mathbf{B})^2}{8m_e^3 c^2} \quad (3.13)$$

$$- \frac{e^2\hbar}{4m_e^2} \frac{\mu_0}{4\pi} g_e \sum_K Z_K \frac{\mathbf{s}_i \cdot (\mathbf{r}_{iK} \times \boldsymbol{\pi}_i)}{r_{iK}^3}, \quad (3.14)$$

contains the NR Coulomb attraction between electron and nuclei (3.10), the relativistic one-electron Darwin correction (3.11) to (3.10) (due to the smearing out of the charge of electron caused by Zitterbewegung of the electron), the NR kinetic and spin-Zeeman interaction (3.12), the relativistic correction to the former (3.13), and the one-electron relativistic spin-orbit coupling term (3.14), where  $\mathbf{r}_{iK} = \mathbf{r}_i - \mathbf{R}_K$  is the position vector of electron relative to nucleus  $K$ . Here  $e$  is positive elementary charge. The two-electron part is composed of

$$h_{ij} = \frac{e^2}{4\pi\epsilon_0} \frac{1}{r_{ij}^2} \quad (3.15)$$

$$- \frac{e^2\hbar^2}{8\epsilon_0 m_e^2 c^2} \delta(\mathbf{r}_{ij}) \quad (3.16)$$

$$- \frac{e^2\hbar}{2m_e^2 c} \frac{\mu_0}{4\pi} g_e \frac{\mathbf{s}_i \cdot [(\mathbf{r}_{ij} \times \boldsymbol{\pi}_i) - 2(\mathbf{r}_{ij} \times \boldsymbol{\pi}_j)]}{r_{ij}^3} \quad (3.17)$$

$$+ \frac{e^2\hbar^2}{4m_e^2} \frac{\mu_0}{4\pi} g_e^2 \left[ \frac{r_{ij}^2 (\mathbf{s}_i \cdot \mathbf{s}_j) - 3(\mathbf{s}_i \cdot \mathbf{r}_{ij})(\mathbf{r}_{ij} \cdot \mathbf{s}_j)}{r_{ij}^5} \right. \quad (3.18)$$

$$\left. - \frac{8\pi}{3} \delta(\mathbf{r}_{ij})(\mathbf{s}_i \cdot \mathbf{s}_j) \right] \quad (3.19)$$

$$- \frac{e^2}{2m_e^2} \frac{\mu_0}{4\pi} \left[ \boldsymbol{\pi}_i \cdot \frac{\boldsymbol{\pi}_j}{r_{ij}} + \frac{(\boldsymbol{\pi} \cdot \mathbf{r}_{ij})(\mathbf{r}_{ij} \cdot \boldsymbol{\pi}_j)}{r_{ij}^3} \right], \quad (3.20)$$

where  $\mathbf{r}_{ij} = \mathbf{r}_i - \mathbf{r}_j$  is the relative position vector of the two electrons. Term (3.15) is the Coulomb repulsion between electrons, (3.16) the two-electron Darwin correction to the former, (3.17) the two-electron spin-orbit interaction containing both

the spin-same orbit (from the Dirac Hamiltonian) and spin-other orbit (from the Breit correction) terms, (3.18) and (3.19) the electronic dipolar and contact type spin-spin interactions, respectively, and (3.20) the relativistic orbit-orbit correction to the two-electron Coulomb interaction. As the electronic contributions on magnetic properties are in focus in present thesis, effects due to external electric fields are neglected here.

### 3.3 Contributions to NMR parameters

The motivation for the approximate methods for calculations of NMR parameters instead of carrying out fully relativistic four-component Dirac-Fock calculations [35, 36, 37, 38] is the high computational expense arising from the four-component character of the latter. In addition, while in the relativistic DF level the actual calculation of magnetic properties is easier due to the single hyperfine operator [39, 40] instead of the many appearing in NR theory (below), the different contributions in the one- and two-component methods give additional insight into the relative importance of the different physical mechanisms.

The Breit-Pauli Hamiltonian (3.9) is the most commonly used level of taking into account relativistic effects on NMR parameters [41, 42, 43, 44, 45]. Its advantages are the numerous existing implementations and ease of interpretation in terms of NR concepts. However, it is not variationally stable and hence only perturbational use is appropriate, although the method of using the frozen core approximation and small basis set in the core overlay region of the valence orbitals, enables doing variational calculations [42, 46]. In this case, however, the NR hyperfine operators are used together with a mass-velocity and Darwin corrected relativistic wave function making the procedure theoretically somewhat dubious. Many of the terms of the BP Hamiltonian are highly singular restricting its perturbational expansion to first order. One solution to this is provided by direct perturbation theory [47], which leads to non-singular expansion. There also exist variationally stable one- and two-component methods such as those provided by zeroth-order regular approximation (ZORA) [48, 49, 50, 51, 52] and Douglas-Kroll (DK) [53, 54, 55] Hamiltonians for carrying out relativistic calculations of NMR parameters.

The first systematic study of all the leading-order relativistic contributions to NMR parameters arising from the BP Hamiltonian is in progress [56]. Hence, only the contributions examined earlier are introduced here. It is essential to accommodate the minimal substitution (3.3) already at the four-component level and carry it through the FW transformation. Otherwise, important contributions will be missing when arriving at the BP level. The interesting magnetic operators are then obtained by substituting  $\boldsymbol{\pi} = -i\hbar\nabla + e\mathbf{A}_0 + e\mathbf{A}_K + e\mathbf{A}_L$  and  $\mathbf{B} = \mathbf{B}_0 + \mathbf{B}_K + \mathbf{B}_L$  to Eq. (3.9), where the external ( $\mathbf{A}_0$ ) and nuclear ( $\mathbf{A}_K$  and  $\mathbf{A}_L$ )

magnetic vector potentials are, in the Coulomb gauge with  $\nabla \cdot \mathbf{A} = 0$ ,

$$\mathbf{A}_0(\mathbf{r}_i) = \frac{1}{2} \mathbf{B}_0 \times \mathbf{r}_{iO}, \quad (3.21)$$

$$\mathbf{A}_K(\mathbf{r}_i) = \hbar \frac{\mu_0}{4\pi} \gamma_K \frac{\mathbf{I}_K \times \mathbf{r}_{iK}}{r_{iK}^3}, \quad (3.22)$$

where  $\mathbf{r}_{iO} = \mathbf{r}_i - \mathbf{R}_O$  is the electronic position vector relative to the gauge origin  $O$ . The magnetic flux density caused by the magnetic vector potential of point-like model for the nuclear magnetic dipole moment (3.22) is [57]

$$\mathbf{B}_K = \mathbf{B}_K^{\text{dip}} + \mathbf{B}_K^{\text{con}(0)} \quad (3.23)$$

$$\mathbf{B}_K^{\text{dip}} = \hbar \frac{\mu_0}{4\pi} \gamma_K \frac{3\mathbf{r}_{iK}\mathbf{r}_{iK} - \mathbf{1}r_{iK}^2}{r_{iK}^5} \cdot \mathbf{I}_K \quad (3.24)$$

$$\mathbf{B}_K^{\text{con}(0)} = \frac{8\pi}{3} \hbar \frac{\mu_0}{4\pi} \gamma_K \delta(\mathbf{r}_{iK}) \mathbf{I}_K. \quad (3.25)$$

The NMR properties are then obtained by gathering all operator combinations bilinear in  $\mathbf{I}_K \mathbf{B}_0$  [up to  $\mathcal{O}(\alpha^4)$  in the fine structure constant] for  $\boldsymbol{\sigma}$  and  $\mathbf{I}_K \mathbf{I}_L$  [up to  $\mathcal{O}(\alpha^6)$ ] for  $\mathbf{J}$ . Since in closed-shell systems the reference is singlet, the triplet operators containing the electronic spin ( $\mathbf{s}_i$ ) should appear in pairs.

The contributions on NMR properties arising from the  $\pi_i^2$  term in Eq. (3.12) are the orbital Zeeman interaction (OZ)

$$\begin{aligned} H^{\text{OZ}} &= \frac{e}{2m_e} \sum_{\epsilon} h_{\epsilon}^{\text{OZ}} B_{0,\epsilon}; \\ h_{\epsilon}^{\text{OZ}} &= \sum_i \ell_{iO,\epsilon}, \end{aligned} \quad (3.26)$$

the paramagnetic nuclear spin – electron orbit interaction (PSO)

$$\begin{aligned} H_K^{\text{PSO}} &= \frac{e\hbar}{m_e} \frac{\mu_0}{4\pi} \gamma_K \sum_{\epsilon} h_{K,\epsilon}^{\text{PSO}} I_{K,\epsilon}; \\ h_{K,\epsilon}^{\text{PSO}} &= \sum_i \frac{\ell_{iK,\epsilon}}{r_{iK}^3}, \end{aligned} \quad (3.27)$$

the diamagnetic shielding interaction (DS)

$$\begin{aligned} H_K^{\text{DS}} &= \frac{e^2 \hbar}{2m_e} \frac{\mu_0}{4\pi} \gamma_K \sum_{\epsilon\tau} h_{K,\epsilon\tau}^{\text{DS}} B_{0,\epsilon} I_{K,\tau}; \\ h_{K,\epsilon\tau}^{\text{DS}} &= \sum_i \frac{(\mathbf{r}_{iO} \cdot \mathbf{r}_{iK}) \delta_{\epsilon\tau} - r_{iK,\epsilon} r_{iO,\tau}}{r_{iK}^3}, \end{aligned} \quad (3.28)$$

and the diamagnetic nuclear spin – electron orbit interaction (DSO)

$$\begin{aligned} H_{KL}^{\text{DSO}} &= \frac{e^2 \hbar^2}{2m_e} \left( \frac{\mu_0}{4\pi} \right)^2 \gamma_K \gamma_L \sum_{\epsilon\tau} h_{KL,\epsilon\tau}^{\text{DSO}} I_{K,\epsilon} I_{L,\tau}; \\ h_{KL,\epsilon\tau}^{\text{DSO}} &= \sum_i \frac{(\mathbf{r}_{iK} \cdot \mathbf{r}_{iL}) \delta_{\epsilon\tau} - r_{iL,\epsilon} r_{iK,\tau}}{r_{iK}^3 r_{iL}^3}. \end{aligned} \quad (3.29)$$

The substitution of the dipole (3.24) and contact (3.25) parts of the magnetic flux density of nucleus into the  $e\hbar g_e \mathbf{s}_i \cdot \mathbf{B}$  term in Eq. (3.12), results in the spin-dipole (SD)

$$\begin{aligned} H_K^{\text{SD}} &= \frac{1}{2} \frac{e\hbar^2}{m_e} \frac{\mu_0}{4\pi} g_e \gamma_K \sum_{\epsilon\tau} h_{K,\epsilon\tau}^{\text{SD}} I_{K,\tau}; \\ h_{K,\epsilon\tau}^{\text{SD}} &= \sum_i \frac{3r_{iK,\epsilon} r_{iK,\tau} - \delta_{\epsilon\tau} r_{iK}^2}{r_{iK}^5} s_{i,\epsilon} \end{aligned} \quad (3.30)$$

and Fermi contact (FC) interactions

$$\begin{aligned} H_K^{\text{FC}} &= \frac{4\pi}{3} \frac{e\hbar^2}{m_e} \frac{\mu_0}{4\pi} g_e \gamma_K \sum_{\epsilon} h_{K,\epsilon}^{\text{FC}} I_{K,\epsilon}; \\ h_{K,\epsilon}^{\text{FC}} &= \sum_i \delta(\mathbf{r}_{iK}) s_{i,\epsilon}. \end{aligned} \quad (3.31)$$

The minimal substitution on the relativistic one- (3.14) and two-electron (3.17) SO terms induces the field-free SO interactions

$$\begin{aligned} H^{\text{SO}} &= \frac{e^2 \hbar}{4m_e^2} \frac{\mu_0}{4\pi} g_e \sum_{\epsilon} \left[ h_{\epsilon}^{\text{SO}(1)} - h_{\epsilon}^{\text{SO}(2)} \right]; \\ h_{\epsilon}^{\text{SO}(1)} &= \sum_K Z_K \sum_i \frac{\ell_{iK,\epsilon}}{r_{iK}^3} s_{i,\epsilon} \end{aligned} \quad (3.32)$$

$$h_{\epsilon}^{\text{SO}(2)} = \sum_K Z_K \sum_{ij}' \frac{\ell_{ij,\epsilon}}{r_{ij}^3} (s_{i,\epsilon} + 2s_{j,\epsilon}), \quad (3.33)$$

as well as the magnetic-field dependent SO interactions arising from either the vector potential of the external magnetic field (3.21)

$$\begin{aligned} H_{B_0}^{\text{SO}} &= \frac{e^3 \hbar}{8m_e^2} \frac{\mu_0}{4\pi} g_e \sum_{\epsilon\tau} \left[ h_{B_0,\epsilon\tau}^{\text{SO}(1)} - h_{B_0,\epsilon\tau}^{\text{SO}(2)} \right] B_{0,\epsilon}; \\ h_{B_0,\epsilon\tau}^{\text{SO}(1)} &= \sum_L Z_L \sum_i \frac{(\mathbf{r}_{iL} \cdot \mathbf{r}_{iO}) \delta_{\epsilon\tau} - r_{iO,\epsilon} r_{iL,\tau}}{r_{iL}^3} s_{i,\epsilon} \end{aligned} \quad (3.34)$$

$$h_{B_0,\epsilon\tau}^{\text{SO}(2)} = \sum_{ij}' \frac{(\mathbf{r}_{ij} \cdot \mathbf{r}_{iO}) \delta_{\epsilon\tau} - r_{iO,\epsilon} r_{ij,\tau}}{r_{ij}^3} s_{i,\epsilon}, \quad (3.35)$$

or the nucleus (3.22)

$$H_K^{\text{SO}} = \frac{e^3 \hbar^2}{4m_e^2} \left( \frac{\mu_0}{4\pi} \right)^2 g_e \gamma_K \sum_{\epsilon\tau} \left[ h_{K,\epsilon\tau}^{\text{SO}(1)} - h_{K,\epsilon\tau}^{\text{SO}(2)} \right] I_{K,\epsilon};$$

$$h_{K,\epsilon\tau}^{\text{SO}(1)} = \sum_L Z_L \sum_i \frac{(\mathbf{r}_{iL} \cdot \mathbf{r}_{iK}) \delta_{\epsilon\tau} - r_{iK,\epsilon} r_{iL,\tau}}{r_{iK}^3 r_{iL}^3} s_{i,\epsilon} \quad (3.36)$$

$$h_{K,\epsilon\tau}^{\text{SO}(2)} = \sum_{ij}' \frac{(\mathbf{r}_{ij} \cdot \mathbf{r}_{iK}) \delta_{\epsilon\tau} - r_{iK,\epsilon} r_{ij,\tau}}{r_{ij}^3 r_{iK}^3} s_{i,\epsilon}, \quad (3.37)$$

called gauge-correction terms [27]. Usually, it is appropriate to neglect the two-electron relativistic corrections, as magnetic properties are dominated by one-electron effects [36, 58].

### 3.3.1 Contributions to spin-spin coupling

It is practical to sort the operator combinations linear both in  $\mathbf{I}_K$  and  $\mathbf{I}_L$  and, hence, contributing to  $\mathbf{J}_{KL}$ , into non-relativistic (NR), spin-orbit (SO), and scalar relativistic (SR) contributions

$$J_{KL,\epsilon\tau} = J_{KL,\epsilon\tau}^{\text{NR}} + J_{KL,\epsilon\tau}^{\text{SO}} + J_{KL,\epsilon\tau}^{\text{SR}}, \quad (3.38)$$

where the five different terms affecting the NR spin-spin coupling tensor are known since Ramsey [5]

$$J_{KL,\epsilon\tau}^{\text{NR}} = J_{KL,\epsilon\tau}^{\text{DSO}} + J_{KL,\epsilon\tau}^{\text{PSO}} + J_{KL,\epsilon\tau}^{\text{SD}} + J_{KL,\epsilon\tau}^{\text{FC}} + J_{KL,\epsilon\tau}^{\text{SD/FC}}. \quad (3.39)$$

The most straightforward to calculate is the ground-state expectation value of the second-order diamagnetic nuclear spin – electron orbit operator (3.29)

$$J_{KL,\epsilon\tau}^{\text{DSO}} = \frac{1}{2\pi} \hbar \gamma_K \gamma_L \frac{e^2}{2m_e} \left( \frac{\mu_0}{4\pi} \right)^2 \langle 0 | h_{KL,\epsilon\tau}^{\text{DSO}} | 0 \rangle \quad (3.40)$$

It provides a typically modest contribution to  $\mathbf{J}$ , sometimes due to the cancellation with the PSO term [See Eq. (3.42) below].

The other NR contributions, represented schematically in Fig. 3.1, arising from the first-order (in either  $\mathbf{I}_K$  or  $\mathbf{I}_L$ ) perturbations  $H_{K,\epsilon}^{(1)} = A_{K,\epsilon}^{(1)} I_{K,\epsilon}$  and  $H_{L,\tau}^{(1)} = C_{L,\tau}^{(1)} I_{L,\tau}$ , are introduced using analytical linear response functions [59, 60] for the second-order perturbation theory expression [5]

$$\langle\langle A_{K,\epsilon}^{(1)}; C_{L,\tau}^{(1)} \rangle\rangle_0 = \sum_{m \neq 0} \frac{\langle 0 | A_{K,\epsilon}^{(1)} | m \rangle \langle m | C_{L,\tau}^{(1)} | 0 \rangle + \langle 0 | C_{L,\tau}^{(1)} | m \rangle \langle m | A_{K,\epsilon}^{(1)} | 0 \rangle}{E_0 - E_m}, \quad (3.41)$$

where the subscript zero means that the frequencies of the both perturbations are zero, *i.e.* perturbations are static. In response theory, all the excited states are implicitly included in the calculation of the analytical derivative and, hence, only

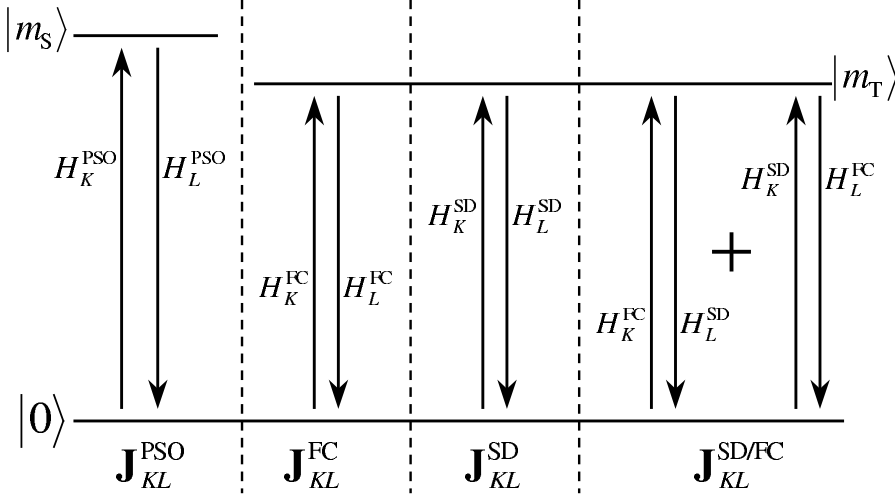


**Figure 3.1.** Schematic illustration of the non-relativistic second-order processes contributing to the nuclear spin-spin coupling tensor.

the ground state wave function is explicitly optimized.

$$J_{KL,\epsilon\tau}^{\text{PSO}} = \frac{1}{2\pi} \hbar \gamma_K \gamma_L \frac{e^2}{m_e^2} \left( \frac{\mu_0}{4\pi} \right)^2 \langle \langle h_{K,\epsilon}^{\text{PSO}}; h_{L,\tau}^{\text{PSO}} \rangle \rangle_0 \quad (3.42)$$

$$J_{KL,\epsilon\tau}^{\text{SD}} = \frac{1}{2\pi} \hbar \gamma_K \gamma_L \frac{1}{4} \frac{e^2 \hbar^2}{m_e^2} \left( \frac{\mu_0}{4\pi} \right)^2 g_e^2 \sum_{\nu=x,y,z} \langle \langle h_{K,\epsilon\nu}^{\text{SD}}; h_{L,\tau\nu}^{\text{SD}} \rangle \rangle_0 \quad (3.43)$$

$$J_{KL,\epsilon\epsilon}^{\text{FC}} = \frac{1}{2\pi} \hbar \gamma_K \gamma_L \frac{16\pi^2}{9} \frac{e^2 \hbar^2}{m_e^2} \left( \frac{\mu_0}{4\pi} \right)^2 g_e^2 \langle \langle h_{K,\epsilon}^{\text{FC}}; h_{L,\epsilon}^{\text{FC}} \rangle \rangle_0 \quad (3.44)$$

$$J_{KL,\epsilon\tau}^{\text{SD/FC}} = \frac{1}{2\pi} \hbar \gamma_K \gamma_L \frac{2\pi}{3} \frac{e^2 \hbar^2}{m_e^2} \left( \frac{\mu_0}{4\pi} \right)^2 g_e^2 \times \left[ \langle \langle h_{K,\epsilon\tau}^{\text{SD}}; h_{L,\tau}^{\text{FC}} \rangle \rangle_0 + \langle \langle h_{L,\tau\epsilon}^{\text{SD}}; h_{K,\epsilon}^{\text{FC}} \rangle \rangle_0 \right] \quad (3.45)$$

Whereas the PSO operator (3.27) couples the closed-shell singlet ground-state with singlet excited electronic states,  $|m\rangle = |m_S\rangle$ , the SD (3.30) and FC operators (3.31) contain electron spin, which induces coupling with triplet excited states,  $|m\rangle = |m_T\rangle$ . The DSO, PSO, and SD terms contribute to the complete tensor [See Eq. 2.18], while the isotropic FC operators only affect the  $J_{KL}\mathbf{1}$  part. The traceless cross-term (SD/FC) contributes only to  $\mathbf{J}_{KL}^S$ . Usually,  $\mathbf{J}^{\text{FC}}$  and  $\mathbf{J}^{\text{FC/SD}}$

are the most important contributions to  $J_{KL}\mathbf{1}$  and  $\mathbf{J}_{KL}^S$ , respectively. The  $\mathbf{J}^{\text{PSO}}$  term may, however, become dominant when the  $s$ -character of the bond between the atoms with the coupled nuclei, is small. Hence, the contribution from the FC operator (3.31) diminishes. In these cases, also the otherwise often small pure SD contribution (3.43) could play an important role.

Relativistic SO effects on  $\mathbf{J}$ , arising from the mixing of the singlet ground state with triplet excited states by the SO interaction, can be classified into third-order,  $J_{KL,\epsilon\tau}^{\text{SO-I}}$ , and second-order,  $J_{KL,\epsilon\tau}^{\text{SO-II}}$ , perturbation theory contributions [45, 61, 62]

$$J_{KL,\epsilon\tau}^{\text{SO}} = \overbrace{J_{KL,\epsilon\tau}^{\text{FC/PSO(1\&2)}} + J_{KL,\epsilon\tau}^{\text{SD/PSO(1\&2)}}}^{=J_{KL,\epsilon\tau}^{\text{SO-I}}} + \overbrace{J_{KL,\epsilon\tau}^{\text{FC/SO(1\&2)}} + J_{KL,\epsilon\tau}^{\text{SD/SO(1\&2)}}}^{=J_{KL,\epsilon\tau}^{\text{SO-II}}}. \quad (3.46)$$

The third-order perturbation theory expression for the  $J_{KL,\epsilon\tau}^{\text{SO-I}}$  corrections can be written as analytical quadratic response functions [59, 63]

$$\langle\langle A_{K,\epsilon}^{(1)}; H^{\text{SO}(n)}, C_{L,\tau}^{(1)} \rangle\rangle_{0,0} = \sum_{m,n \neq 0} \frac{\langle 0|A_{K,\epsilon}^{(1)}|m\rangle \langle m|H^{\text{SO}(n)}|n\rangle \langle n|C_{L,\tau}^{(1)}|0\rangle + \text{permut.}}{(E_0 - E_m)(E_0 - E_n)}, \quad (3.47)$$

where, in addition to the first-order operators  $H_{K,\epsilon}^{(1)}$  and  $H_{L,\tau}^{(1)}$ , the zeroth-order (including neither  $\mathbf{I}_K$  nor  $\mathbf{B}_0$ ), one- (3.32) and two-electron (3.33) field-free SO operators appear. Each of the four third-order SO corrections [45, 61, 62]

$$J_{KL,\epsilon\tau}^{\text{FC/PSO}(n)} = \frac{1}{2\pi} \hbar \gamma_K \gamma_L \frac{\pi e^4 \hbar^2}{3 m_e^4} \left(\frac{\mu_0}{4\pi}\right)^3 g_e^2 \left[ \langle\langle h_{K,\epsilon}^{\text{FC}}; h_{\epsilon}^{\text{SO}(n)}, h_{L,\tau}^{\text{PSO}} \rangle\rangle_{0,0} + \langle\langle h_{L,\tau}^{\text{FC}}; h_{\tau}^{\text{SO}(n)}, h_{K,\epsilon}^{\text{PSO}} \rangle\rangle_{0,0} \right] \quad (3.48)$$

$$J_{KL,\epsilon\tau}^{\text{SD/PSO}(n)} = \frac{1}{2\pi} \hbar \gamma_K \gamma_L \frac{1 e^4 \hbar^2}{8 m_e^4} \left(\frac{\mu_0}{4\pi}\right)^3 g_e^2 \sum_{\nu=x,y,z} \left[ \langle\langle h_{K,\epsilon\nu}^{\text{SD}}; h_{\nu}^{\text{SO}(n)}, h_{L,\tau}^{\text{PSO}} \rangle\rangle_{0,0} + \langle\langle h_{L,\tau\nu}^{\text{SD}}; h_{\nu}^{\text{SO}(n)}, h_{K,\epsilon}^{\text{PSO}} \rangle\rangle_{0,0} \right] \quad (3.49)$$

have an effect on the complete  $\mathbf{J}_{KL}$  tensor. The  $(n)$  denotes one- (1) or two-electron (2) SO operator. Here, the singlet excited state is coupled by PSO to one and FC or SD operators couple the triplet state to the other nucleus [45, 61, 62]. The third-order processes are illustrated in Fig. 3.2 on page 30.

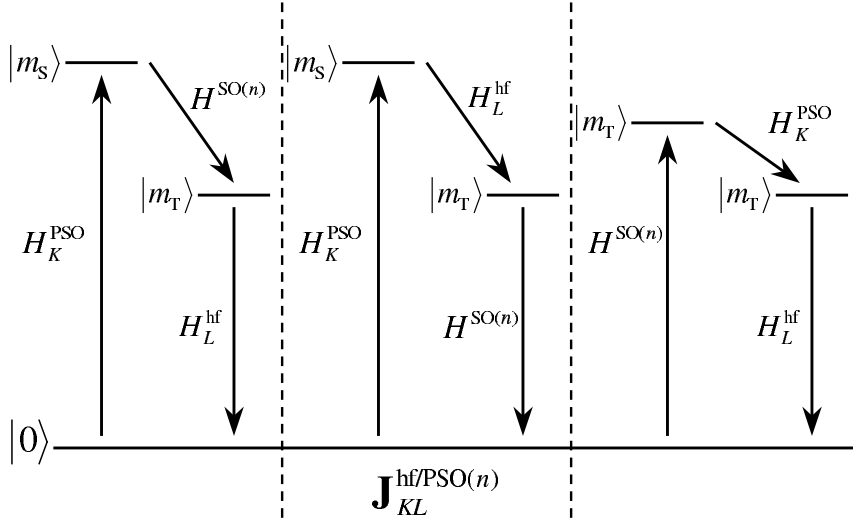


**Figure 3.2.** Schematic illustration of the relativistic third-order spin-orbit processes contributing to the nuclear spin-spin coupling tensor. The hf denotes either (hyperfine) FC or SD operator.

The second-order SO contributions [45]

$$J_{KL,\epsilon\tau}^{\text{FC}/\text{SO}(n)} = \frac{1}{2\pi} \hbar \gamma_K \gamma_L \frac{\pi}{3} \frac{e^4 \hbar^2}{m_e^3} \left( \frac{\mu_0}{4\pi} \right)^3 g_e^2 \left[ \langle \langle h_{K,\epsilon}^{\text{FC}}; h_{L,\tau\epsilon}^{\text{SO}(n)} \rangle \rangle_0 + \langle \langle h_{L,\tau}^{\text{FC}}; h_{K,\epsilon\tau}^{\text{SO}(n)} \rangle \rangle_0 \right] \quad (3.50)$$

$$J_{KL,\epsilon\tau}^{\text{SD}/\text{SO}(n)} = \frac{1}{2\pi} \hbar \gamma_K \gamma_L \frac{1}{8} \frac{e^4 \hbar^2}{m_e^3} \left( \frac{\mu_0}{4\pi} \right)^3 g_e^2 \sum_{\nu=x,y,z} \left[ \langle \langle h_{K,\epsilon\nu}^{\text{SD}}; h_{L,\tau\nu}^{\text{SO}(n)} \rangle \rangle_0 + \langle \langle h_{L,\tau\nu}^{\text{SD}}; h_{K,\epsilon\nu}^{\text{SO}(n)} \rangle \rangle_0 \right] \quad (3.51)$$

are due to the coupling through triplet excited state [See *e.g.* the SD/FC process in Fig. 3.1 on page 28.] induced by the FC or SD operators in one nucleus and the one- (3.36) and two-electron (3.37) SO operators including the magnetic vector potential of the nucleus [27, 45] for the other nucleus. Both the  $J_{KL,\epsilon\tau}^{\text{SO-I}}$  and  $J_{KL,\epsilon\tau}^{\text{SO-II}}$  contributions are of  $\mathcal{O}(\alpha^6)$  and contribute to the complete  $\mathbf{J}$  tensor. The SO corrections are, as expected, highly dependent on the one-electron basis set in both core and valence regions [45]. They are the main relativistic contributions to light atom couplings in systems containing heavy atoms, whereas the relativistic effects

for couplings with heavy atom itself are mainly due to the SR effects [38, 50] and the SO corrections are very small [45]. In order to obtain quantitative agreement with experiment, the inclusion of SR corrections on  $\mathbf{J}$  have been shown by the ZORA DFT method to be important due to the relativistic increase of  $J^{\text{FC}}$  caused by the core tails of valence orbitals [10, 50]. The study of relativistic effects based on  $H_{\text{BP}}$  is in progress [56, 64].

### 3.3.2 Contributions to shielding

The BP Hamiltonian terms linear both in  $\mathbf{I}_K$  and/or  $\mathbf{B}_0$  give rise to the nuclear shielding tensor  $\sigma_K$ . As in the case of  $\mathbf{J}_{KL}$ , the contributions to  $\sigma_K$  can be divided into NR, SO, and SR parts:

$$\sigma_{K,\epsilon\tau} = \sigma_{K,\epsilon\tau}^{\text{NR}} + \sigma_{K,\epsilon\tau}^{\text{SO}} + \sigma_{K,\epsilon\tau}^{\text{SR}}. \quad (3.52)$$

In closed-shell molecules,  $\sigma_K^{\text{NR}}$  contains two contributions [6, 7]:

$$\sigma_{K,\epsilon\tau}^{\text{NR}} = \sigma_{K,\epsilon\tau}^{\text{d}} + \sigma_{K,\epsilon\tau}^{\text{p}}, \quad (3.53)$$

where the diamagnetic shielding  $\sigma_K^{\text{d}}$  is a ground-state expectation value of the second-order operator in Eq. (3.28)

$$\sigma_{K,\epsilon\tau}^{\text{d}} = \frac{e^2 \hbar \mu_0}{2m_e} \frac{1}{4\pi} \gamma_K \langle 0 | h_{K,\epsilon\tau}^{\text{DS}} | 0 \rangle. \quad (3.54)$$

The second-order paramagnetic shielding term

$$\sigma_{K,\epsilon\tau}^{\text{p}} = \frac{e^2 \hbar \mu_0}{2m_e^2} \frac{1}{4\pi} \gamma_K \langle \langle h_{K,\epsilon}^{\text{PSO}}; h_{\tau}^{\text{OZ}} \rangle \rangle_0, \quad (3.55)$$

can be expressed as a linear response function (3.41) of the PSO (3.27) (first-order in  $\mathbf{I}_K$ ) and OZ (3.26) (first-order in  $\mathbf{B}_0$ ) contributions [See the singlet process in Fig. 3.1 on page 28.]. As the operators in both  $\sigma_K^{\text{d}}$  and  $\sigma_K^{\text{p}}$  contain  $\mathbf{r}_{iO} = \mathbf{r}_i - \mathbf{R}_O$ , they depend on the choice of  $\mathbf{R}_O$ . The experimental observable does not depend on this choice and therefore the sum of  $\sigma_K^{\text{d}}$  and  $\sigma_K^{\text{p}}$  should be gauge-independent. This is not a problem in atoms where the natural choice is the position of nuclei  $\mathbf{R}_O = \mathbf{R}_K$ . In addition, due to the spherically symmetric electronic distribution,  $\sigma_K^{\text{p}} = \mathbf{0}$  and hence  $\sigma_K^{\text{NR}} = \sigma_K^{\text{d}}$ . In molecules, however, the choice of the gauge origin is crucial and several methods have been developed to make the sum of the computed dia- and paramagnetic contributions gauge invariant. These methods make the wave function dependent on the external magnetic field by including gauge terms either at the molecular orbital level in methods called localized orbital/local origin (LORG) [65] or individual gauges for localized orbitals (IGLO) [66, 67], or at the atomic orbital level in the gauge-including atomic orbital

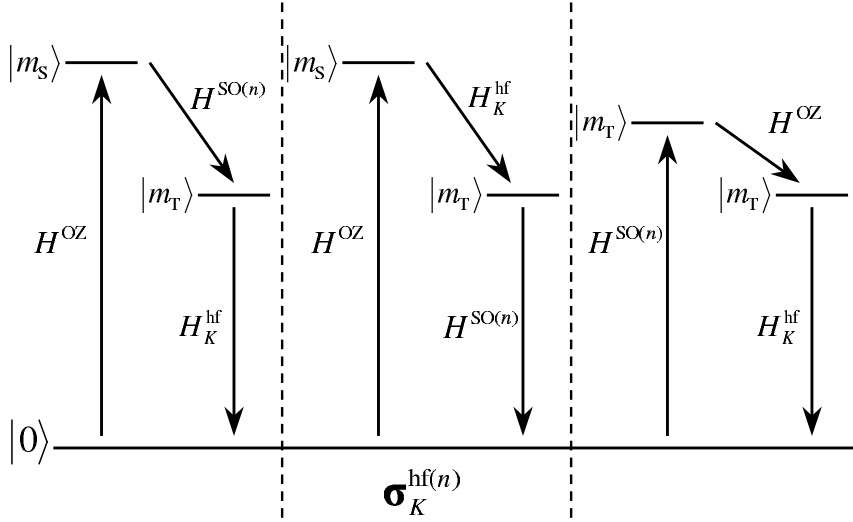


**Figure 3.3.** Schematic illustration of the relativistic third-order spin-orbit processes contributing to the nuclear shielding tensor. The hf denotes either (hyperfine) FC or SD operator.

(GIAO) [68, 69, 70, 71] method. However, at the complete basis set limit, also the use of common gauge origin (CGO) provides gauge independent results.

There are both third-order,  $\sigma_{K,\epsilon\tau}^{\text{SO-I}}$ , and second-order,  $\sigma_{K,\epsilon\tau}^{\text{SO-II}}$ , relativistic SO contributions also to nuclear shielding

$$\sigma_{K,\epsilon\tau}^{\text{SO}} = \underbrace{\sigma_{K,\epsilon\tau}^{\text{SO-I}}}_{=\sigma_{K,\epsilon\tau}^{\text{SO-I}}} = \underbrace{\sigma_{K,\epsilon\tau}^{\text{FC(1\&2)}} + \sigma_{K,\epsilon\tau}^{\text{SD(1\&2)}}}_{=\sigma_{K,\epsilon\tau}^{\text{SO-I}}} + \underbrace{\sigma_{K,\epsilon\tau}^{\text{FC-II(1\&2)}} + \sigma_{K,\epsilon\tau}^{\text{SD-II(1\&2)}}}_{=\sigma_{K,\epsilon\tau}^{\text{SO-II}}}, \quad (3.56)$$

where  $\sigma_{K,\epsilon\tau}^{\text{SO-I}}$  is due to the field-free one- (3.32) and two-electron (3.33) SO operators that couple either the singlet ground or singlet excited state to triplet excited state. In the former, the mixing between triplet excited states is due to the OZ operator (3.26) and the coupling back to ground state is provided by either the FC (3.31) or SD (3.30) interactions. The OZ operator is also responsible for mixing of the singlet ground and excited states in the latter case [43, 44]. All processes are presented in the Fig. 3.3.

$$\sigma_{K,\epsilon\tau}^{\text{FC}(n)} = \frac{4\pi e^4 \hbar^3}{3} \left(\frac{\mu_0}{8m_e^4}\right)^2 \frac{1}{(4\pi)} g_e^2 \gamma_K \langle\langle h_{K,\epsilon}^{\text{FC}}; h_{\epsilon}^{\text{SO}(n)}, h_{\tau}^{\text{OZ}} \rangle\rangle_{0,0} \quad (3.57)$$

$$\sigma_{K,\epsilon\tau}^{\text{SD}(n)} = \frac{1}{2} \frac{e^4 \hbar^3}{8m_e^4} \left(\frac{\mu_0}{4\pi}\right)^2 g_e^2 \gamma_K \sum_{\nu=x,y,z} \langle\langle h_{K,\epsilon\nu}^{\text{SD}}; h_{\nu}^{\text{SO}(n)}, h_{\tau}^{\text{OZ}} \rangle\rangle_{0,0}. \quad (3.58)$$

The FC(1) contribution is the most significant for light atom shielding and the one-electron terms appears to have greater significance than the two-electron contributions. However, all the third-order SO corrections should be included in accurate calculations, particularly of heavy element shieldings as the degree of cancellation varies from system to other [43, 44].

The second-order contributions

$$\sigma_{K,\epsilon\tau}^{\text{FC-II}(n)} = \frac{4\pi e^4 \hbar^3}{3} \frac{1}{8m_e^3} \left(\frac{\mu_0}{4\pi}\right)^2 g_e^2 \gamma_K \langle\langle h_{K,\epsilon}^{\text{FC}}; h_{B_0,\tau\epsilon}^{\text{SO}(n)} \rangle\rangle_0 \quad (3.59)$$

$$\sigma_{K,\epsilon\tau}^{\text{SD-II}(n)} = \frac{1}{2} \frac{e^4 \hbar^3}{8m_e^3} \left(\frac{\mu_0}{4\pi}\right)^2 g_e^2 \gamma_K \sum_{\nu=x,y,z} \langle\langle h_{K,\epsilon\nu}^{\text{SD}}; h_{B_0,\tau\nu}^{\text{SO}(n)} \rangle\rangle_0, \quad (3.60)$$

where the triplet excited state due to the FC or SD operators is coupled back to singlet ground state by external magnetic-field dependent one- (3.34) and two-electron (3.35) SO operators [See the triplet processes in Fig. 3.1 on page 28.], appear to be the dominant SO effects for the heavy atom shieldings, though only the one-electron parts were studied [41, 44]. As  $\sigma_{K,\epsilon\tau}^{\text{SO-II}}$  makes the total SO effect gauge-invariant, it is also called the gauge correction term. Excluding all SO terms involving the SD operator is usually an appropriate approximation, since the FC terms are the dominating ones [43, 44, 72]. Both  $\sigma_{K,\epsilon\tau}^{\text{SO-I}}$  and  $\sigma_{K,\epsilon\tau}^{\text{SO-II}}$  contribute to the rank-0, -1, and -2 parts of  $\sigma_K$ .

As in the case of  $\sigma_K^{\text{p}}$  in the NR shielding, the third-order  $\sigma_{K,\epsilon\tau}^{\text{SO-I}}$  contribution containing the OZ operator is zero by symmetry in closed-shell atoms as well as in the bond direction in linear molecules (paramagnetic contribution), and the only contributing term is the second-order  $\sigma_{K,\epsilon\tau}^{\text{SO-II}}$  (diamagnetic contribution) [44]. Although the NR shielding is often quite well-described already at the SCF level (as electron correlation effects are not large), the third-order SO corrections necessitate the use of a method that is stable against triplet excitations, implying the need for a good correlated method. However, the second-order SO contribution appears to be quite insensitive to correlation. Both  $\sigma_{K,\epsilon\tau}^{\text{SO-I}}$  and  $\sigma_{K,\epsilon\tau}^{\text{SO-II}}$  necessitate basis set with enough flexibility in core region for the atom in question, in order to reach basis set convergence [43, 44]. Both the one- and two-electron SO operator integrals in  $\sigma_{K,\epsilon\tau}^{\text{SO-I}}$  are well-approximated by the Breit-Pauli one-electron/one-center mean-field approximation [73, 74] and hence can be calculated very efficiently using *e.g.* the AMFI code [75].

The SO effects do not cover all the relativistic effects on shielding. The importance of spin-free relativistic effects, SR effects, becomes large towards heavier nuclei [38, 46, 52]. One of the important relativistic contributions, provided by the FC mechanism interacting with the relativistic kinetic energy correction to the

spin Zeeman interaction [38, 76], cannot be straightforwardly classified as either SR or SO effect. However, since the operator in Eq. (3.13) gives rise to various other relativistic terms [41, 55] that are still not thoroughly explored, a project is in progress where the purpose is to cover also the other relativistic contributions from the BP Hamiltonian (3.9) [56, 76].

## 4 Computation of spin-spin coupling

In this Chapter the aim is to discuss the level of theoretical calculations necessary for accurate description of the spin-spin coupling tensor  $\mathbf{J}$ . As mentioned earlier,  $\mathbf{J}$  constitutes very interesting object for theoretical molecular physics research as it is highly dependent on the quality of the basis set, electron correlation, and relativistic effects. Here we concentrate on the two former effects, leaving the last one for future examination, together with rovibrational and solvent effects. Due to its contribution to the experimentally observed dipole coupling in anisotropic LC and solid state environments, the results from the computation of anisotropic part of  $\mathbf{J}$  are reviewed thoroughly.

### 4.1 Summary of the papers

The Papers I, II, and III are concerned with the reliable determination of the anisotropic properties of the  $\mathbf{J}$  tensor both experimentally and theoretically. The main motivation is to study the relative importance of the anisotropic contribution  $\frac{1}{2}J_{KL}^{\text{aniso}}$ , to the experimentally observed anisotropic dipolar coupling  $D_{KL}^{\text{exp}}$  (2.20) that is used for obtaining structural and/or orientational information of the molecule. In Paper I, the couplings involving carbon and hydrogen in differently bonded simple hydrocarbons,  $\text{C}_2\text{H}_2$ ,  $\text{C}_2\text{H}_4$ , and  $\text{C}_2\text{H}_6$ , were examined, completing the study started with benzene,  $\text{C}_6\text{H}_6$  [77]. Paper II deals with couplings involving also silicon, in addition to carbon and hydrogen, in methylsilane,  $\text{CH}_3\text{SiH}_3$ . The transferability and relative magnitude of the carbon and silicon coupling tensors between similar molecules, ethane (Paper I) and methylsilane (Paper II), were also scrutinized. The non-negligible  $\frac{1}{2}J_{KL}^{\text{aniso}}$  contributions to  $D_{KL}^{\text{exp}}$  including fluorine found for *para*-difluorobenzene [78] inspired an exploration of fluorine couplings in simple fluoromethanes,  $\text{CH}_3\text{F}$ ,  $\text{CH}_2\text{F}_2$ , and  $\text{CHF}_3$ , in Paper III. The contributions from the CC, CH, and HX ( $X = \text{H}, \text{F}, \text{Si}$ ) tensors were found to be negligible while the  ${}^1\mathbf{J}_{\text{CSi}}$  contribute significantly to  ${}^1D_{\text{CSi}}^{\text{exp}}$ . The effects of the both CF and FF couplings can be neglected with reasonable accuracy in  $D_{KL}^{\text{exp}}$  couplings in fluoromethanes. However, the results in *para*-difluorobenzene [78] and difluoromethane

(Paper III) suggest that particularly the FF coupling might have a notable effect due to the low symmetry  $\mathbf{J}_{KL}$  in the direction between coupled nuclei.

From the computational point of view, the Papers I, II, and III provide information about the conditions for accurate computational determination of  $\mathbf{J}$ . The description of one-electron orbitals in the form of basis sets, as well as the effects arising from the electron-electron interaction are studied in detail for both  $\mathbf{J}$  and  $\sigma$  tensors by using MCSCF theory. The MCSCF electron correlation treatment is studied further in Paper IV, concentrating on the core-valence correlation (CVC) effects that were suspected to be the reason for the somewhat lower than usual quality of results obtained for CSi coupling in Paper II. In Paper IV, CVC together with other correlation effects were studied for both  $\mathbf{J}$  and  $\sigma$  in first- and second-row main-group hydrides with the aim to provide recommendation of the necessary level of correlation treatment.

In Papers I–IV, MCSCF is shown to provide reliable  $\mathbf{J}$  tensors when very large active spaces, preferably of multireference type, are used in order to include enough dynamical and static correlation. Also CVC effects arising from semicore orbitals are necessary to accommodate in couplings involving second-row elements. This is not needed for  $\sigma$  due to markedly smaller CVC effect (Paper IV).

In Paper V, the performance of DFT in producing reliable  $\mathbf{J}$  was investigated, with the different exchange-correlation functional types, local-density approximation (LDA) [79], generalized gradient approximation (GGA) using gradient corrected Becke–Lee–Yang–Parr (BLYP) functional [80, 81], as well as hybrid three-parameter Becke–Lee–Yang–Parr (B3LYP) [82, 83] functional. The focus was on the anisotropic properties. The explored systems were the same as in previous Papers I–IV and other MCSCF studies concerning FHF<sup>-</sup> (Paper V), C<sub>6</sub>H<sub>6</sub> [77], *p*-C<sub>6</sub>H<sub>4</sub>F<sub>2</sub> [78], HCONH<sub>2</sub> [84], diatomic [85], ClF<sub>3</sub> and OF<sub>2</sub> [86], as well as HCN, HNC, CH<sub>3</sub>CN, CH<sub>3</sub>NC molecules [87]. The same geometries and basis set as in MCSCF calculations were used for all molecules. DFT with the hybrid B3LYP functional was shown to provide reasonably accurate  $\mathbf{J}$  tensors including first- and second-row elements other than halogens.

## 4.2 One-electron basis set

The sensitivity of  $\mathbf{J}$  to the quality of the basis set is due to the many contributing physical mechanisms that probe the immediate vicinity of the nucleus and are transmitted through the electron structure to the other nucleus. The former fact, when using the point-like nuclear model, necessitates a good fulfillment of the nuclear cusp condition, *i.e.* the wave function should have an exponential behavior at the nucleus. This demands a balanced one-electron description where both the core and valence basis sets are flexible enough. In practice, this means that at least a polarized triple-zeta (TZ) and preferably a quadruple-zeta (QZ) basis set should be used

The correlated wave function methods, such as MCSCF and coupled-cluster (CC) [3, 88, 89], place additional demands for the basis set. To describe dynamical

Table 4.1. Primary basis sets used in the present calculations.<sup>a</sup>

Atom	HII	HIII	HIV
H	[5s 1p/3s 1p]	[6s 2p/4s 2p]	[6s 3p 1d/5s 3p 1d]
C-F	[9s 5p 1d/5s 4p 1d]	[11s 7p 2d/7s 6p 2d]	[11s 7p 3d 1f/8s 7p 3d 1f]
Si-Cl	[11s 7p 2d/7s 6p 2d]	[12s 8p 3d/8s 7p 3d]	[12s 8p 4d 2f/9s 8p 4d 2f]
Se <sup>b</sup>	[16s 13p 10d/11s 10p 10d]	[16s 13p 11d/12s 11p 11d]	[16s 13p 12d 2f/13s 12p 12d 2f]
Te <sup>b</sup>	[20s 16p 13d/13s 12p 10d]	[20s 16p 14d/14s 13p 12d]	[20s 16p 15d 2f/15s 14p 14d 2f]

<sup>a</sup> In the [primitive/contracted] notation. Only the innermost orbitals of each type are contracted. Spherical Gaussian functions are used throughout. <sup>b</sup> Basis set of Fægri [99] used with same type of contraction pattern and polarization functions as in the basis sets for the lighter elements.

correlation well, one needs extra flexibility in both angular and radial directions. There exist basis set families that are constructed for correlated calculations, *e.g.* atomic natural orbitals (ANO) [90, 91, 92] and correlation consistent basis sets cc-pVXZ etc. [93, 94]. When used with correlated methods, these basis sets provide consistent behavior of the total electronic energy of the molecule with respect to the improvement of the basis set. In the basis set study for spin-spin coupling constants, Helgaker *et al.* [95] found that the cc-pVXZ-*sun* series of correlated consistent basis sets, provides smooth convergence and comparable accuracy with the much larger cc-pCVXZ [93, 96] and aug-cc-pCVXZ [94] basis sets. In cc-pVXZ-*sun* series, the *s* functions of cc-pVXZ basis are fully decontracted and a sequence of *n* tight *s* functions with the exponents forming a geometrical progression, are added.

Consistently with the experience gained in Papers I–IV, Helgaker *et al.* [95] found also that the basis set series of Huzinaga [97], modified by Kutzelnigg *et al.* [98] and denoted HII, HIII, and HIV, produce well-converged spin-spin couplings, particularly when considering the modest size of these sets. Although HII–HIV were not systematically constructed with respect to the recovery of electron correlation energy, they seem to provide a good compromise for the less complete correlation methods. The advantage is that they are much smaller than the correlation-consistent sets and provide reasonable flexibility in the core region. Therefore good results with two largest sets, HIII and HIV, can be achieved. The HII, HIII, and HIV basis sets are described in Table 4.1. Our choice has been to use these compact sets in the present applications.

The basis set convergence of isotropic and symmetric anisotropic parts (and, of course, antisymmetric parts) of the **J** tensor is in principle unequal as they consist of different combinations of the several physical contributions. When relativistic effects are taken into account, the demands placed on the description of the orbitals become even greater. The addition of only *s* functions may not be sufficient enough but one also needs to add tight functions with  $l > 0$  as, *e.g.* the relativistic spin-orbit operator probes also the angular structure of the basis set and not only the radial one.

### 4.3 Many-electron effects

In addition to the substantial requirements for the description at the one-electron level, heavy demands are also placed for the many-electron description by the spin-spin coupling tensor. This is due to the fact that already at the NR level of theory,  $\mathbf{J}$  contains contributions from the triplet FC and SD operators that necessitate correct description of the triplet excitation spectrum and, therefore, many-electron method that does not suffer triplet instability [22]. In other words, electron correlation effects are very important and *post*-Hartree-Fock methods are needed. In the present chapter, general features of electron correlation effects are presented, followed by a discussion of their effects on  $\mathbf{J}$ .

#### 4.3.1 Electron correlation

By electron correlation one means the Coulombic interactions between electrons that are not described by the single-configuration Hartree-Fock approximation [3, 100]. One measure of these effects is the correlation energy of the electron system which is defined as the difference between the exact (NR) and the Hartree-Fock energy,  $E_{\text{corr}} = E_{\text{exact}} - E_{\text{HF}}$  [3], for a given electronic state, where the reference wave function is usually of the restricted Hartree-Fock (RHF) type for closed-shell systems. Strictly speaking this definition is only valid at the complete basis set limit of both calculations, but in practice it is also used with finite basis sets. The Fermi correlation arising from the antisymmetry requirement of the wave function by the Pauli principle is already included in the reference HF wave function.

The electron correlation is usually divided into dynamical and static (also called nondynamical) correlation [3]. Dynamical correlation is due to the instantaneous Coulomb repulsion between electrons. Due to the singular form of the Coulomb operator, it causes the so-called Coulomb hole [3] around the electron in the exact wave function, meaning that the probability amplitude of another electron is shifted away from it. The overall form of this hole, determined by the so-called long-range dynamical correlation, is well-reproduced by relatively small number of many-electron configurations. Methods of including dynamical correlation in the cases where the ground state is dominated by a single HF configuration, are the many-body perturbation theories, such as the second-order Møller-Plesset (MP2) [101, 3], or CC theories. A more severe problem is to describe the short-range dynamical correlation related to the Coulomb cusp. While quite good results are obtained by high-level CC theories including single (S), double (D), and some or all of the triple (T) excitations [CCSD(T), CC3, CCSDT], very high accuracy is only attained by explicitly correlated R12 methods [102].

The near-degeneracy effects arising from the interactions between the Hartree-Fock and other electronic configurations are called static correlation. These effects usually occur when the molecule dissociates. The ground-state wave function can also be of the multireference type already at the equilibrium geometry, either due to the hybridization of the bonds or the presence of a heavy element that has

low-lying excited states. Also the excited states are usually strongly affected by static correlation. Static correlation is handled by including all the dominant as well as nearly degenerate configurations into the calculation. As it is important to handle these configurations on equal footing, a good approximation for static correlation is the MCSCF method where both the one-electron orbitals and the many-electron configuration expansion are optimized at the same time.

One should note, though, that the separation of the static and dynamical correlation is somewhat ambiguous with high-level methods. Especially, this division becomes meaningless when all the correlation with a given basis set is taken into account in the full configuration interaction (FCI) calculation, where all possible electronic configurations with correct spin and spatial symmetries, are included into the configurational expansion. In the CC methods, when higher than double excitations are included, also some of the static correlation effects are practically taken into account. Similarly, when the MCSCF method is extended from the complete active space (CAS) [3, 103] to restricted active space (RAS) [3] wave function, the main dynamical correlation effects can be treated. In the CAS method [See Fig. 4.1 on page 40.], FCI calculation is carried out for a limited active orbital space (usually including only valence orbitals) and the double occupied orbitals in inactive space are optimized but not correlated. The treatment of dynamical correlation in the RAS method [Fig. 4.1] is based on the division of the active space into (usually) three distinct active spaces: in RAS1 (RAS3) the maximum number of holes (particles) can be specified, while RAS2 corresponds to the active space of a CAS calculation, being free of constraints. It is in principle possible to converge the calculation to the FCI limit by both CC and MCSCF methods.

### 4.3.2 *Static and dynamical correlation effects in J*

As the spin-spin coupling tensor includes contributions that couple the ground state with triplet excited states, it is a quite sensitive probe for the quality of the wave function with respect to static correlation. For couplings over double and triple bonds, this is very apparent as observed in the case of  ${}^1J_{CC}$  in  $C_2H_4$  and  $C_2H_2$  (Paper I) as well as previously for couplings, *e.g.* over the aromatic ring in  $C_6H_6$  [77]. Therefore, a qualitative approximation for the correlation effects is already obtained by using a small CAS active space. An easy method of choosing the active space is to use natural occupation numbers (NON) of orbitals *i.e.* eigenvalues of the spin-reduced single particle density matrix obtained from a MP2 calculation, to reveal the significance of individual orbitals in the correlation treatment.

In order to converge the results with respect to dynamical correlation, one needs very large configuration spaces. Hence, it is more suitable to use a RAS-type wave function where in the RAS2 subspace only the occupied valence orbitals are included, while the most important unoccupied orbitals are in the RAS3 subspace. In this way, the active orbital space can be made quite large providing a good description of dynamical correlation. This is a single-reference approximation as

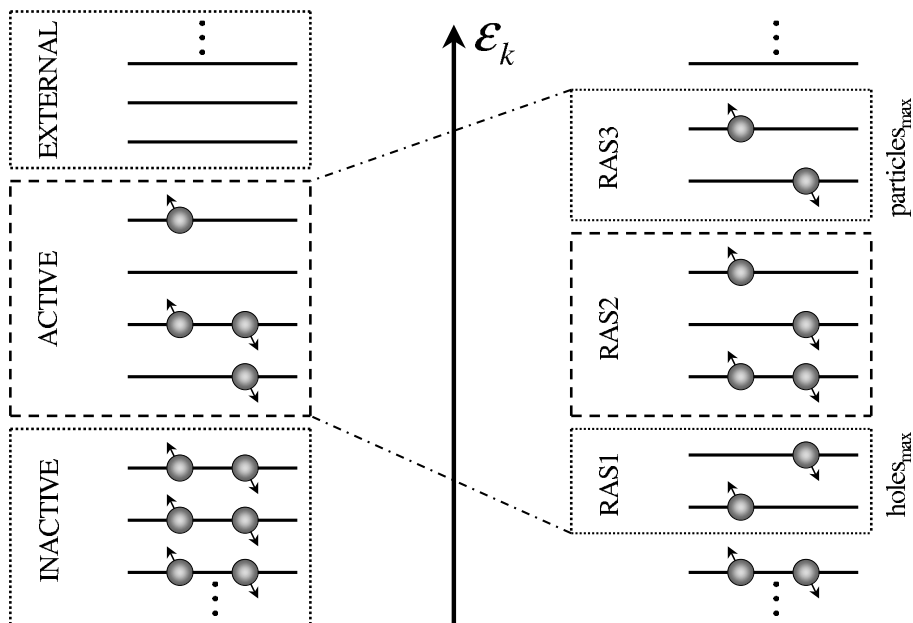


Figure 4.1. Schematic illustration of the CAS (on the left) and RAS (on the right) division of molecular orbitals into subspaces in multiconfigurational self-consistent field calculations. All possible combinations of configurations are constructed within the CAS active space and RAS2, while in RAS1 (RAS3) the maximum number of holes (particles) may be specified.

only the occupied orbitals are included in RAS2 and therefore only one, optimized, reference wave function exists from which excitations are allowed to the virtual orbitals in the RAS3 subspace. The selection of the RAS3 orbitals should be done carefully with a balanced fashion, as discussed for the HF molecule in Paper IV. In practice, the active space is often truncated based on clear gaps in the NONs. The experience gathered in the present studies is that the active space should contain at least 90% and preferably over 95% of the virtual MP2 particles, for quantitative description. The single-reference wave function is observed to produce proper  $\mathbf{J}_{KL}$  in singly bonded systems at the equilibrium geometry (Papers I–IV).

If one needs to account also for the static correlation in the multiply-bonded cases mentioned earlier, or to obtain very accurate  $\mathbf{J}$  tensors in systems containing only single bonds (Paper IV), one can either move one or more of the lowest unoccupied molecular orbitals from RAS3 to RAS2, or allow higher than double excitations from the occupied orbitals to the unoccupied ones (in HF picture). In the latter approach, using up to quadruple excitations from occupied orbitals in

RAS2 to unoccupied ones in RAS3 is found to provide a reasonable approximation for the static correlation effects obtainable otherwise from large multireference calculations (Paper IV) [104]. In Paper IV, it was also apparent that a multireference wave function has an effect mainly on the triplet FC contribution and not on the singlet PSO contribution, in the systems considered. This implies that static “configurational” correlation affects principally the triplet excitation spectrum. This also explains the observations that the anisotropic tensorial properties are even more sensitive to the treatment of static correlation than the isotropic coupling constants (Paper I).

### 4.3.3 Core-valence correlation

As there are various types of hyperfine operators contributing to the  $\mathbf{J}$  tensor, it is anticipated that also electron correlation from the semicore orbitals is important in addition to valence orbitals that usually are correlated in MCSCF calculations. In molecules containing first row elements, this is not a problem since other than the  $1s$  orbitals are typically included in the correlation treatment and the effect of core  $1s$  orbitals is generally found to be negligible (Paper IV). In the next row of the periodic table, the atoms also contain semicore electrons that are found to be important for accurate description of the  $\mathbf{J}$  tensor, especially involving the heavy nucleus but also for hydrogen-hydrogen coupling (Paper IV). These CVC effects on the anisotropic properties are found to be of similar importance but not necessarily to the same direction as in the case of the coupling constants.

A compromise strategy in the inclusion of the different correlation effects with reasonable computational effort is to use a single-reference wave function correlating only the valence orbitals (SR-V2) for  $^1J_{XH}$ , when X is a first row element. This is due to the cancelling multireference and core-correlation effects. However, in the second-row hydrides, a wave function of multireference type, featuring correlation of the semicore orbitals (MR-SC2) is necessary for accurate determination of  $^1J_{XH}$ . These wave functions rapidly become computationally heavy and, hence, the single-reference type wave function in which the semicore orbitals are correlated (SR-SC2) may be a pragmatic approximation. High accuracy for  $^2J_{HH}$  demands multireference wave functions with the semicore correlated, *i.e.* MR-V2 on the first and MR-SC2 on the second row. If unavoidable, the latter can be best approximated by MR-V2.

Jaszuński and Ruud [105] presented a method of approximating the CAS wave function of  $C_2H_2$  by restricting the number of electrons excited from the occupied valence orbitals to four. This is done by moving orbitals to the RAS1 subspace and allowing up to quadruple ( $0 \rightarrow 4$ ) excitations from these orbitals to the other active orbitals (unoccupied in the HF picture). This was found to cause a negligible difference in the description of static correlation, as compared to the corresponding CAS calculation. Hence, it should also be possible to take into account CVC by treating the excitations from the semicore orbitals in this way. Although this would limit the computational effort considerably in comparison with calculations

where all the occupied orbitals are located in the RAS2 subspace, the practical limit for the system size is rapidly reached with MCSCF, especially if heavy atoms are present. Therefore, methods that correlate all electrons on an equal footing such as DFT or *ab initio* approaches (MP2 and CC) (without the frozen core approximation), may be preferable in the long run. In addition, MCSCF is essentially a truncated CI method and, hence, loses the full size-extensivity of the HF method (*i.e.*, the total energy no longer scales linearly with the system size when calculated as a sum of the energies of the identical noninteracting subsystems). Hence, for the computation of large systems, size-extensive methods such as DFT, MP2, or CC, are preferable.

## 4.4 Tensorial properties

The main reason for calculating the anisotropic properties of  $\mathbf{J}_{KL}$  is their contribution,  $\frac{1}{2}J_{KL}^{\text{aniso}}$ , to the experimental anisotropic coupling observed in NMR spectroscopy (2.20). The question is then, whether or not this contribution is generally negligible for a particular type of coupling. Accurate theoretical calculations of the complete  $\mathbf{J}_{KL}$  tensors have been enabled by the quite recently developed *ab initio* methods, the MCSCF linear response (LR) [63], the second-order polarization-propagator approach with CCSD amplitudes [SOPPA(CCSD)] [106], together with its predecessor CCSDPPA [107, 108], and the equations-of-motion CCSD (EOM-CCSD) methods [109, 110, 111]. Also DFT methods [50, 51, 112, 113, 114] are found to provide reasonable  $\mathbf{J}$  tensors. Recent DFT implementations [115, 116] opened possibilities to consistently investigate the  $\mathbf{J}$  tensors in systems of experimentally interesting size. This is a consequence of their generality as they include all the NR contributions analytically and enable the use of each of the three generations of exchange-correlation functionals: LDA, GGA, and hybrid functionals containing part of the exact HF exchange. The recent reviews [10, 22] summarize the methods and their applications.

### 4.4.1 *Ab initio calculations*

Together with CC methods, the most accurate way of calculating the  $\mathbf{J}$  tensors is MCSCF. It has no constraints on whether reference state has a multireference character or not. Also, when using a RAS type MCSCF wave function, it has been shown [77, 84], partly by papers included in this Thesis (IIV), that in practice also dynamical correlation effects can be taken into account at least in small molecules.

In Paper I, the MCSCF LR method is observed to produce reliable  $\mathbf{J}$  for simple hydrocarbons,  $\text{C}_2\text{H}_2$ ,  $\text{C}_2\text{H}_4$ ,  $\text{C}_2\text{H}_6$ , as confirmed by reasonable convergence with respect to both basis set and correlation treatment. Also the good agreement with experimental data supports this conclusion. Also in Paper III, the agreement between the experiment and the MCSCF calculations is found to be excellent for the

fluoromethanes. In the isotropic couplings the compatibility is eminently good and the error in the anisotropic properties is maximally only a few percent. One should keep in mind that the anisotropic properties are experimentally very challenging and, hence, much more inaccurate than the experimental coupling constants. Paper III also demonstrates that, as expected, fluorine causes no particular problem for the MCSCF method, by contrast to the DFT method with the presently available functionals [112, 113, 114]. As observed in the case of trifluoromethane, the correlation treatment affects more the couplings between heavy atoms than the couplings to hydrogen. The couplings involving hydrogen are found to be more sensitive to the description of the single-electron level than the electron correlation treatment. One should still remember that the static correlation effects on hydrogen couplings are important when very accurate results are expected (Paper IV). In Paper II, the coupling tensors of methylsilane other than  ${}^1\mathbf{J}_{\text{CSi}}$ , are described with similar high accuracy as in the two previous studies. The somewhat worse agreement with experiment in this coupling is at least partially due to the neglect of semicore correlation as shown in Paper IV, as the basis set and active space (including only the valence orbitals) used for methylsilane are at least of similar quality as those used for hydrocarbons (Paper I) and fluoromethanes (Paper III). In any case, qualitative picture of the anisotropic part of  ${}^1\mathbf{J}_{\text{CSi}}$  was obtained.

The FC and SD/FC contributions are typically the most significant contributions in the isotropic coupling constants and anisotropic properties, respectively, for ethane (Paper I), methylsilane (Paper II), and fluoromethanes (Paper III). For CH and HH couplings, this is partly due to the cancellation of DSO and PSO terms. In ethene, the FC contribution to  ${}^2J_{\text{HH}}$  is very small. The usually small SD term gives significant contribution to  ${}^1\mathbf{J}_{\text{CC}}$  over multiple bonds and for  ${}^1\mathbf{J}_{\text{CSi}}$ ,  ${}^1\mathbf{J}_{\text{CF}}$ , and  ${}^2\mathbf{J}_{\text{FF}}$  in singly-bonded systems. In couplings involving fluorine, the cancellation of DSO and PSO terms is not as complete usually, due to the significant PSO contributions. Both multiple bonds and lone-pair elements, as well as heavier elements such as Si, increase the relative importance of the DSO, SD, and especially PSO terms as observed also by Bryce and Wasylshen [85]. The DSO term dominates the  $\Delta^3 J_{\text{HH}}$  in ethyne and  $\Delta^2 J_{\text{HH}}$  in diluoromethane. Especially trifluoromethane (Paper III) provides a good example for concluding that one cannot *a priori* neglect any of the different physical contributions to  $\mathbf{J}$ .

In order to compare coupling tensors in different symmetries, the principal axis system (PAS), illustrated for methylsilane in Fig. 4.2 on page 44, may be used for the symmetric part of the tensor ( $J_{KL}\mathbf{1} + \mathbf{J}_{KL}^S$ ). The couplings may furthermore be presented as reduced couplings  $\mathbf{K}_{KL}$  to facilitate comparison of couplings between different nuclei. As observed in Paper II from this kind of analysis, silicon doubles the magnitude of the couplings as compared to carbon. However, both the CH and HH (in methyl groups) coupling constants and anisotropies are very similar in both ethane and methylsilane. Hence, it appears that tensors can be transferred in the molecule-fixed frame from one molecule to another if the local symmetry of the corresponding structural units is similar [117].

In theoretical studies, the choice of the molecular geometry can disturb the comparison with experimental data. Hence, one should be very careful when choosing the structure to be used in calculations. One should preferably use either the

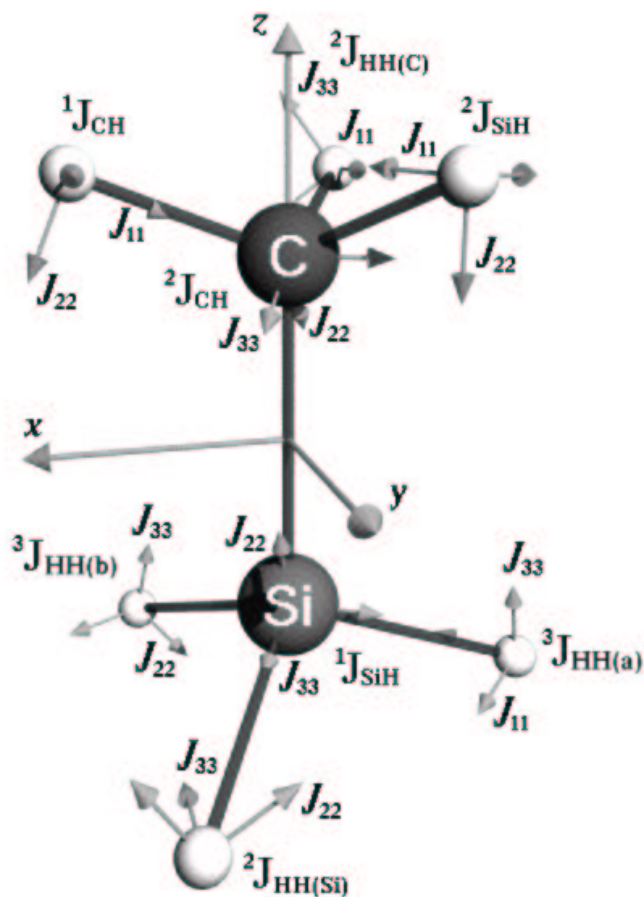


**Figure 4.2.** The principal axis systems of the various spin-spin coupling tensors in methylsilane. The  $x$  axis is in the HCSiH plane, where the protons are the ones for which the PAS of the  $^1J_{CH}$  and  $^3J_{HH(a)}$  tensors are shown (in the respective order).

experimental or theoretical equilibrium geometry,  $r_e$ , and carry out rovibrational averaging at a given temperature for the property in question, to reach comparability with the experimental results obtained in the gas phase. If experiments are carried out in liquid solution as usual, also solvent effects should be modeled. One approximation to the full rovibrational treatment is to use the  $r_\alpha^{0K} = r_z$  geometry that takes the main anharmonic vibrational effects into account [20].

An approximate method of including the effects of molecular vibrations on  $^1J_{CF}$  at 300 K was used for  $CH_3F$  in Paper IV. The method was similar to that used

for the shielding tensor in Paper VI (discussed in Section 5.3) but including only the symmetric first- and second-order bond stretch terms from the approximate Taylor expansion. The result was that these effects do not influence the comparison between experimental and theoretical values drastically. As only the effects from the symmetric bond stretch were included, the Eckart conditions [118] for the geometries displaced from the equilibrium were naturally satisfied. Generally, the tensor elements of  $\mathbf{J}^S$  should be presented in the Eckart frame that rotates with the molecule and minimizes the coupling between vibrational and rotational motion of the molecule [118, 119]. The rovibrational contributions for  $\Delta J$  are typically found to be quite small for systems investigated so far in the literature [10].

For HH and CH couplings, the effect of  $\frac{1}{2}J_{KL}^{\text{aniso}}$  is typically less than 1% and hence it can be generally be neglected when reasonably accurate dipolar couplings are wanted for the determination of structural and/or orientational parameters [8]. As the anisotropic part in CC couplings is less than 1% in simple hydrocarbons (Paper I) and less than 2% in benzene [77], its effect can mostly be neglected. The same is true for CF couplings in singly-bonded fluoromethanes as their effects are typically below 1% (Paper III). However, the CF couplings over the aromatic ring in difluorobenzene have been found to contribute about 3% to the experimental  $D_{\text{CF}}^{\text{exp}}$  couplings [78]. Hence, in the case of fluorine couplings, the  $\frac{1}{2}J_{KL}^{\text{aniso}}$  contribution can not be *a priori* neglected. The case of CSi coupling where the relative contribution of  $\frac{1}{2}J_{\text{CSi}}^{\text{aniso}}$  in the  $D_{\text{CSi}}^{\text{exp}}$  is about 3%, illustrates the increasing trend when the nuclear charge of the coupled nucleus increases [85]. The neglect of an indirect contribution of this size causes an error of 2%...3% for the orientational order parameter  $S_{\text{CSi}}$  and +1% for the  $r_{\text{CSi}}$  bond length (Paper II).

Although the direct dipolar coupling  $D_{KL}$  and indirect spin-spin coupling  $\frac{1}{2}J_{KL}^{\text{aniso}}$  contributions depend similarly on the orientational order parameters, they are not necessarily zero under the same conditions, when the molecule has less than two-fold symmetry and the two tensors are not aligned [10]. This is due to the fact that  $\mathbf{D}_{KL}$  is cylindrically symmetric in the direction of the line between  $K$  and  $L$ , while  $\mathbf{J}_{KL}$  generally is not. Hence, orientations may exist where the direct part nearly vanishes and the observed experimental anisotropic coupling is dominated by the indirect part. In particular, when very small dipolar couplings are used for the determination of the structure of non-symmetric biomolecules, one should also assess the effect of indirect contribution. One way is to use the observed transferability of the tensors.

#### 4.4.2 Density-functional theory calculations

Since the basis sets and molecular geometries are kept the same as in the previous Papers I–IV as well as in the previous MCSCF studies [77, 78, 84, 85, 86, 87], electron correlation effects on  $\mathbf{J}$  are left as the topic for the comparison of methods in Paper V. The results are also compared with experiment but as the rovibrational and solvent effects are not taken into account by the theoretical calculations, the correspondence of theory and experiment can not be expected to be perfect. The

main focus of Paper V is the quality of the anisotropic properties of  $\mathbf{J}$  calculated using the DFT LR method and especially when using, for the first time, a hybrid DFT functional for this purpose. The correlation of DFT and MCSCF data is illustrated for CC, CH, HH, FF, CF, XF, and XY coupling tensors in Figures 4.3–4.6. However, one should keep in mind that the MCSCF data is of benchmark quality only if the correlation treatment is pursued far enough by the RAS method as done in Papers I–IV.

The hybrid B3LYP functional generally performs best among the DFT functionals for all types of couplings. Also, the gradient corrected BLYP functional provides reasonable results, whereas LDA exhibits the least consistent behavior. Especially the  ${}^n\mathbf{J}_{\text{CC}}$  [Fig. 4.3],  ${}^n\mathbf{J}_{\text{CH}}$  [Fig. 4.4abc], and  ${}^n\mathbf{J}_{\text{HH}}$  [Fig. 4.4edf] tensors are described by B3LYP with at least similar accuracy as by MCSCF calculations. This is particularly noteworthy when the system size increases and it is not practical to include enough electron correlation in the the MCSCF wave function, due to the massive computational demands. In CH and HH couplings, the accuracy is even better with DFT than with MCSCF when compared to experimental data. In these couplings the good total  $\mathbf{J}_{KL}$  by DFT arise due to the well-calculated contributions and not due to error cancellation. In systems containing multiple bonds, the individual physical contributions to  ${}^n\mathbf{J}_{\text{CC}}$  arising from the paramagnetic PSO, SD, and FC operators become worse with DFT, resulting in somewhat lower quality total tensors. In addition, when Si, P, S, or N are coupled through single bonds, the complete  $\mathbf{J}_{KL}$  tensors are very accurately calculated by B3LYP. However, caution should be exercised in couplings with oxygen. Again, couplings over multiple bonds are more problematic for DFT, related to the existing problem in describing static correlation by the present DFT functionals optimized for accounting the dynamical correlation. Hence, great hopes are directed towards the ongoing development of local functionals accounting for non-local (exact exchange) effects including static correlation [120].

The real difficulties with DFT arise when couplings involving fluorine are concerned. For isotropic couplings this has been known for long and it has been related to insufficient long-range behavior of the present functionals when lone-pair elements are present [112, 113]. The poor description of spin density for the centers with lone pairs manifest itself in the incorrect FC (SD/FC in anisotropic parts) contributions. The unsatisfactory results, as in the case of  ${}^n\mathbf{J}_{\text{FF}}$  [Fig. 4.5abc], are also affected by the erroneous PSO contributions. The contribution of defective SD is usually much smaller. The occasionally occurring, favorable error cancellation improves the total property; hence B3LYP has some value in estimating the rough magnitude of properties of  ${}^n\mathbf{J}_{\text{FF}}$  in very large systems, where MCSCF no longer is usable. A surprise is provided by the quite good anisotropic properties of  ${}^n\mathbf{J}_{\text{CF}}$  [Fig. 4.5def] while the isotropic coupling behave as badly as in the FF coupling. Partitioning the dominant SD/FC contribution into individual terms SD(F)/FC(C) and SD(C)/FC(F) clearly illustrates the reason for the good results. The large relative error in the small term arising when the FC operator is located at the fluorine, SD(C)/FC(F), is over-compensated by the much larger but well-calculated SD(F)/FC(C) contribution in the leading SD/FC contribution to the anisotropic coupling. When the dominance of the SD/FC term is not present,

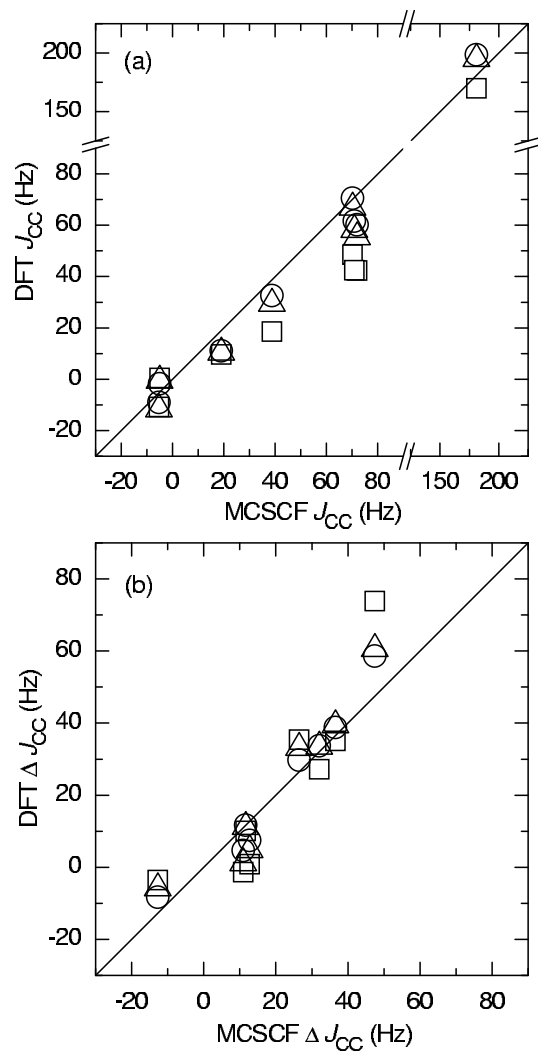


**Figure 4.3. Properties of the  $J_{CC}$  tensor by DFT and MCSCF. (a) Coupling constants  $J_{CC}$  by LDA ( $\square$ ), BLYP ( $\triangle$ ), and B3LYP ( $\circ$ ) functionals. (b) Anisotropies  $\Delta J_{CC}$ .**

the errors in the other (particularly PSO) contributions settle the result further away from both MCSCF and experimental values. The favorable error cancellation of PSO with FC and SD/FC contributions works well for the  ${}^nJ_{FH}$  tensors by B3LYP, with some exceptions (HF and FHF<sup>-</sup>).

The couplings involving alkali atoms in diatomic molecules, some including also

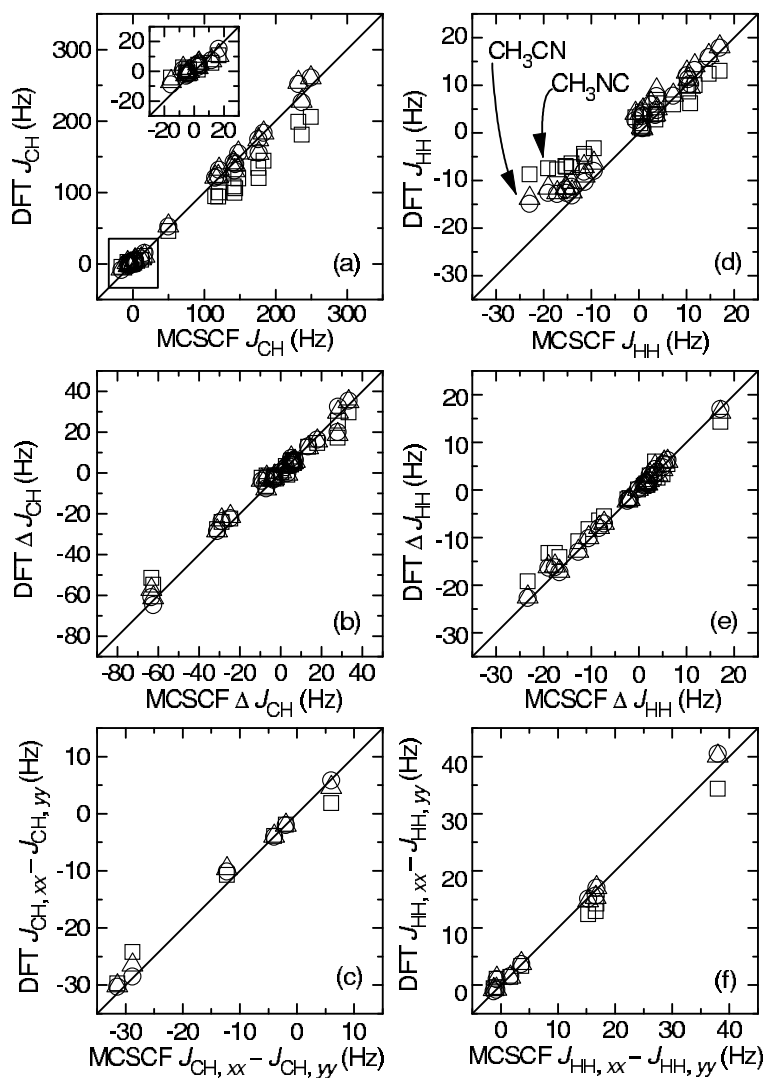


**Figure 4.4.** Properties of the  $J_{\text{CH}}$  and  $J_{\text{HH}}$  tensors by DFT and MCSCF. (a) Coupling constants  $J_{\text{CH}}$ , (b) anisotropies  $\Delta J_{\text{CH}}$ , (c) asymmetry  $J_{\text{CH},xx} - J_{\text{CH},yy}$ , (d)  $J_{\text{HH}}$ , (e)  $\Delta J_{\text{HH}}$ , and (f)  $J_{\text{HH},xx} - J_{\text{HH},yy}$ . Symbols as in Figure 4.3.

fluorine [Fig. 4.6], are described by B3LYP with the same accuracy as with modest CAS calculations [85]. Where experimental data exists, both methods are seen to have problems. This is expected, as DFT suffers from the same problems as with halogens (in the case of alkali atoms there are several unoccupied valence orbitals). With a modest CAS active space, dynamical correlation effects are poorly

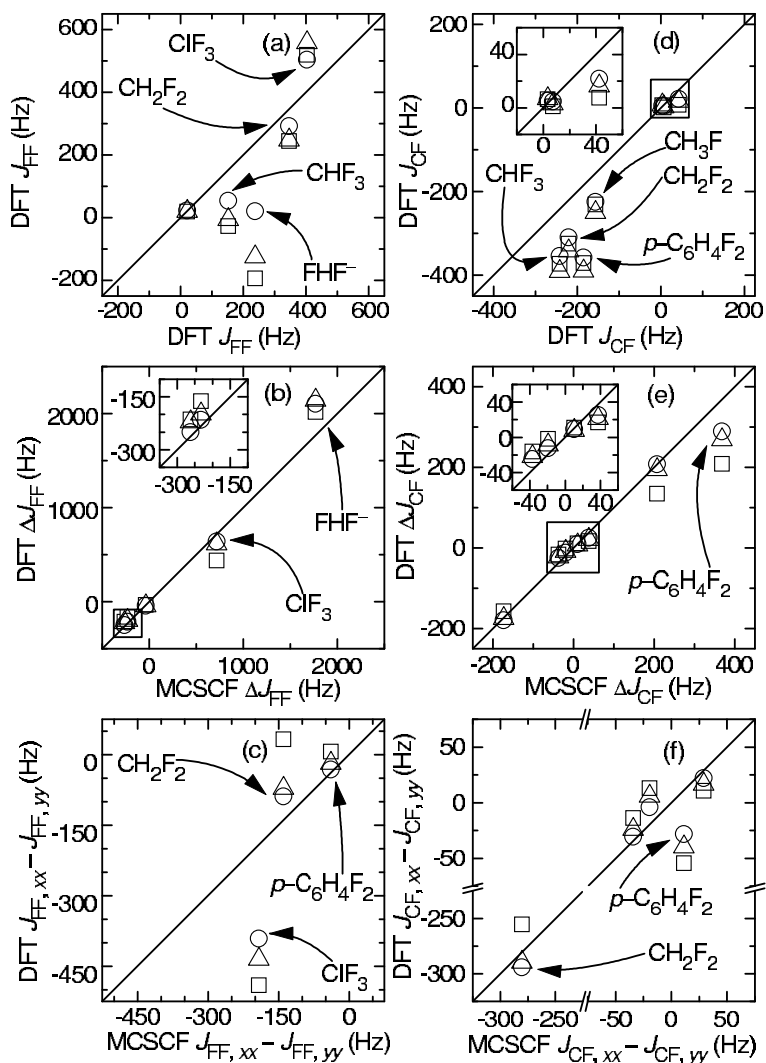


**Figure 4.5.** Properties of the  $J_{FF}$  and  $J_{CF}$  tensors by DFT and MCSCF. (a) Coupling constants  $J_{FF}$ , (b) anisotropies  $\Delta J_{FF}$ , (c) asymmetry  $J_{FF,xx} - J_{FF,yy}$ , (d)  $J_{CF}$ , (e)  $\Delta J_{CF}$ , and (f)  $J_{CF,xx} - J_{CF,yy}$ . Symbols as in Figure 4.3.

recovered. Couplings to halogen elements other than fluorine are, expectedly, also difficult for DFT with all functionals. Caution should be exercised also with the DFT method for the generally well-behaving couplings, *e.g.*  $\mathbf{J}_{XY}$  in systems where several troublesome (especially F) atoms exist. For instance, the  $^1J_{CH}$  in  $\text{CHF}_3$  is of unusually low quality.

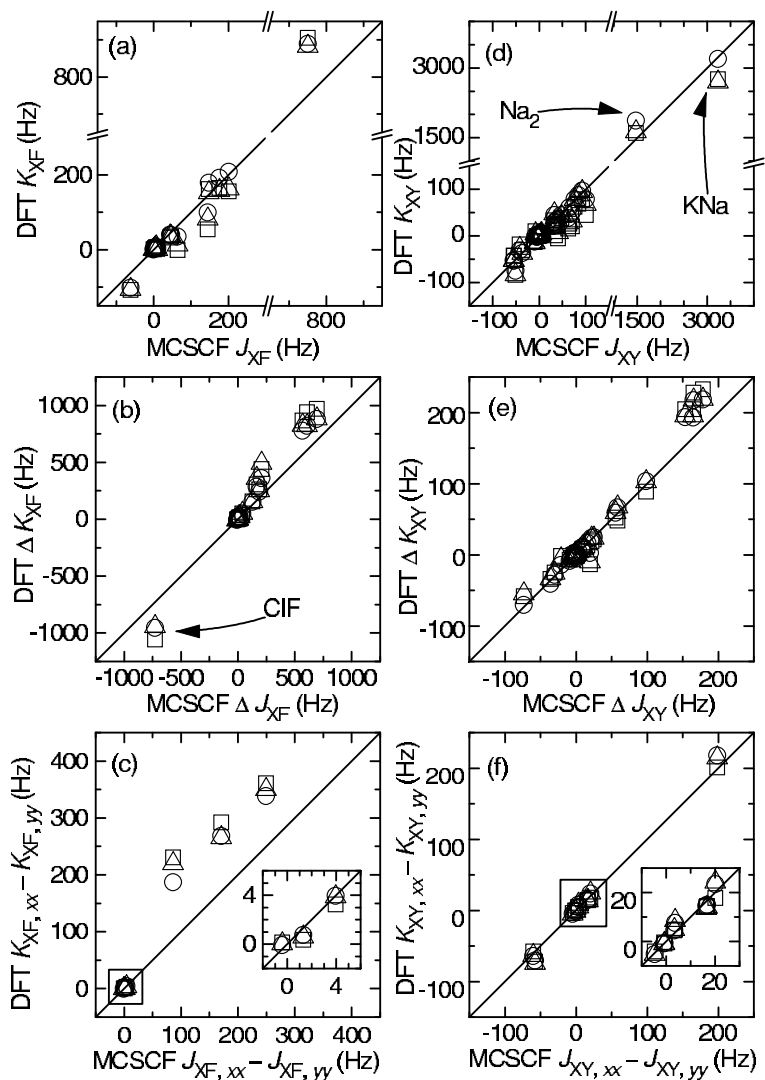


**Figure 4.6.** Properties of the  $J_{XF}$  and  $J_{XY}$  tensors by DFT and MCSCF. (a) Coupling constants  $J_{XF}$ , (b) anisotropies  $\Delta J_{XF}$ , (c) asymmetry  $J_{XF,xx} - J_{XF,yy}$ , (d)  $J_{XY}$ , (e)  $\Delta J_{XY}$ , and (f)  $J_{XY,xx} - J_{XY,yy}$ . Symbols as in Figure 4.3.

In a recent study [121],  $J^{\text{PSO}}$  (and nuclear shielding constant) were observed to be improved by using self-interaction correction (SIC) at the LDA level. It was noted by the authors that the same improvement was not reached for the  $J^{\text{FC}}$  term; even deterioration of the results was observed. The authors of Ref. [10]

suggest that the neglect of the response of the SIC potential to the magnetic field might be one reason for this. In any case, this direction of functional development is very welcome as there is a need for a systematic improvement of the exchange-correlation functionals based on new physical ideas.

The hybrid B3LYP functional, in the context of DFT LR method, provides **J** tensors with reasonable accuracy in most couplings. Quantitative results can be obtained at least for couplings between carbon and hydrogen atoms. As the DFT method is size-extensive, the accuracy remains the same also in large systems. Hence, the capability of DFT surpasses those of MCSCF in large systems. This, together with its high computational efficiency makes it very promising in applications concerning **J** tensors in large bio- and organic molecules.

However, one should remember that, with the present exchange-correlation functionals, DFT cannot be considered as *ab initio* method in the sense that convergence of the different properties with respect to systematic improvement of the electron correlation treatment, could in principle be monitored without either prior knowledge of the system, or experimental data. The motivation for developing correlated methods such as MCSCF and CC arises out of their ability to produce information independent of experiments. Hence, they can also serve as benchmarks for more approximate but computationally expedient methods, such as DFT.

## 5 Computation of shielding

The nuclear shielding tensor  $\sigma$  is the most often examined NMR property by quantum chemical methods. In addition to the basis set and correlation requirements of  $\sigma$ , discussed already in Papers I and IV, Paper VI concentrates on the secondary isotope shifts, *i.e.* chemical shifts of the nucleus arising from the change of isotopes of other nuclei in the system, on carbon shielding in  $CX_2$  ( $X = O, S, Se, \text{ and } Te$ ) systems. This necessitates taking into account the vibrational and rotational motions of the molecule. The rovibrational treatment for  $\sigma$  in Paper VI could also be applied to  $J$ . In systems containing heavy nuclei, the relativistic SO effects play an important role in the shielding of both heavy and light nuclei. The SO effects on the finite temperature rovibrational corrections on  $\sigma_C$  are found to be significant in Paper VI. On this account, also the secondary isotope shifts and their temperature effects are highly dependent on the SO contributions and the previously noted discrepancy between experiment and NR calculations is fully explained by them, hence the motivation for Paper VI.

### 5.1 One- and many-electron description

At the NR level, the basis set demands of the  $\sigma$  are two-fold. A reasonable accuracy is usually obtained already using the HIII basis set and HIV is practically converged for main group elements (Paper I) [84]. However, as already mentioned in Section 3.3.2, uncontracting and augmenting the basis set with tight functions is necessary in order to obtain converged relativistic SO corrections to the  $\sigma$ .

Although the  $\sigma^{NR}$  is not as sensitive to electron correlation treatment as  $J$  due to absence of triplet contributions – even HF wave function occasionally gives reasonable results – there are still significant correlation effects present when quantitative accuracy is expected [122, 123]. This is evident also from the study of the simple hydrocarbons in Paper I by the GIAO MCSCF method [124], where the small RAS active space was observed to overshoot the correlation effects in carbon shielding and much larger active orbital space was needed for convergence. A multireference wave function is necessary for systems with multiple bonds. The

CVC effects are quite small and can be neglected for general purposes, as observed in Paper IV. In order to obtain highly accurate  $\sigma$ , multireference wave functions are needed, especially in the case of the anisotropic properties that appear to be more sensitive to static correlation than the isotropic shielding constants. An occasionally occurring cancellation between static (multireference wave function) and dynamical (extension of the active space) correlation effects diminishes the computational demands. In any case, the GIAO MCSCF method provides at least qualitatively correct shielding parameters and constitutes a systematic method of reaching correlation convergence.

The MCSCF accuracy for  $\sigma$  is, for other than simplest systems, easily exceeded by the GIAO CCSD [122], and GIAO CCSD(T) [123] methods, which efficiently recover most of the dynamical and also some part of static correlation effects. The latter method results in benchmark accuracy in most cases. The MP2 perturbation theory method allows a quite good approximate way of including correlation for  $\sigma$  as it usually overshoots the dynamical and neglects static correlation effects resulting in favorable cancellation of correlation effects. Due to the low computational cost compared to MCSCF and CCSD(T), also basis set convergence is easier to reach. An even more cost-efficient method is to use DFT with GIAOs, which have been found to have potential for providing nuclear shielding constants of promising quality [125, 126, 127, 128]. Despite this, the accuracy of the DFT method is not known *a priori* and, hence, accurate *ab initio* calculations are necessary for calibration purposes.

## 5.2 Spin-orbit corrections to carbon shielding

As mentioned in Section 3.3.2, relativistic SO effects are very important for light atom shielding in systems containing heavy atoms [43, 44, 72, 129]. An increasing deviation between results obtained for both NR and SO shieldings in Paper VI, when going towards heavier molecules, indicates difficulties in accounting for electron correlation by either the MCSCF active spaces or the present exchange-correlation functionals of DFT. The neglect of semicore correlation in the MCSCF wave functions used, can affect especially the SO corrections that include FC and SD operators (Paper IV). The NR shieldings may also be affected by the quite small active spaces. The DFT method has been known to produce good relative chemical shifts [125, 126, 127, 130] but absolute nuclear shieldings suffer from the approximate exchange-correlation functionals. The often occurring deshielding is also present in the study of Paper VI. The main cause for the smaller SO corrections by the DFT is the FC(1) term, which is, together with FC(2), quite dependent on electron correlation effects. In addition, the use of CGO at carbon instead of the IGLO gauge brings the DFT SO values closer to the MCSCF results.

The positive and negative SO corrections on  $^{13}\text{C}$  shielding constant and anisotropy, respectively, increase when the X nuclei become heavier, as expected. The third-order (SO-I) contribution is always the dominant one and the second-order (SO-II) term diminishes the total magnitude of the SO contribution as shown in

Tables 2 and 3 of Paper VI. The SO correction brings the calculated shieldings into very good agreement with the experimental value in CSe<sub>2</sub> molecule. Also the <sup>13</sup>C shielding in the other heavy-atom molecule, CTe<sub>2</sub>, is very dependent on the SO correction, resulting in positive shielding constant, contrary to the negative ones in CS<sub>2</sub> and CSe<sub>2</sub>. However, as the DFT value is positive and there are no experimental results, the sign of  $\sigma_C$  in CTe<sub>2</sub> remains an open question. One interesting observation is also that  $\Delta\sigma_C$  in CTe<sub>2</sub> is smaller than in CS<sub>2</sub> and CSe<sub>2</sub> due to the SO correction. The total  $\sigma_K$  by the DFT and MCSCF are of similar quality due to the cancellation of differences.

### 5.3 Rovibrational corrections and isotope effects

It is assumed that reasonably accurate shielding surfaces near the equilibrium geometry can be obtained with DFT, enabling sufficient description of the temperature dependence of both the absolute shieldings  $\sigma_C$  and the secondary isotope shifts  $-\langle\sigma_C(M'X)\rangle - \langle\sigma_C(MX)\rangle$ , where  $M$  and  $M'$  are the mass numbers of the different isotopes of the neighboring nucleus X ( $M' > M$ ).

In Paper VI, rovibrational averaging at temperature  $T$  is carried out for the <sup>13</sup>C shielding constant by expanding the shielding a Taylor series in terms of the internal displacement coordinates  $\Delta R_i$  *i.e.* bond lengths and angles around the equilibrium geometry value  $\sigma_e$

$$\begin{aligned} \langle\sigma\rangle^T &= \sigma_e + \sigma_r [\langle\Delta r\rangle^T + \langle\Delta r'\rangle^T] + \frac{1}{2}\sigma_{rr} [\langle(\Delta r)^2\rangle^T + \langle(\Delta r')^2\rangle^T] \\ &+ \sigma_{rr'} \langle\Delta r \Delta r'\rangle^T + \frac{1}{2}\sigma_{\theta\theta} [\langle(\Delta\theta)^2\rangle^T + \langle(\Delta\theta')^2\rangle^T]. \end{aligned} \quad (5.1)$$

The first ( $\sigma_{R_i}$ ) and second ( $\sigma_{R_i R_j}$ ) derivatives of the property, taken at the equilibrium geometry, are obtained from the calculated shielding surface around the equilibrium. As the first and second derivatives of scalar properties are independent of temperature and nuclear masses in the Born-Oppenheimer approximation,<sup>1</sup> they can be calculated from the shielding surface around the equilibrium geometry. The temperature and nuclear mass dependence is included in the isotropic case in the thermal averages of displacement magnitudes,  $\langle\Delta R_i\rangle^T$  and  $\langle\Delta R_i \Delta R_j\rangle^T$ . To calculate these to leading order, the (quadratic) harmonic,  $f_{R_i R_j}$ , and (cubic) anharmonic force field,  $f_{R_i R_j R_k}$ , are needed. The evaluation of the thermal averages for each isotopomers individually is carried out using the rectilinear vibrational normal coordinate basis,  $Q_k$ , resulting in the normal coordinate averages  $\langle Q_k\rangle^T$  and  $\langle Q_k^2\rangle^T$ . While the latter average only includes harmonic vibrations, the former is affected by both vibration and rotation (through centrifugal distortion) of the molecule [131, 132].

The combined effect of the opposite NR (negative) and SO (positive) rovibrational contributions on <sup>13</sup>C nuclear shielding is that the magnitude of the total

<sup>1</sup>When anisotropic properties are investigated, the molecule-fixed Eckart frame has to be used for representing the property, and the mass dependence of the orientation of the frame is therefore reflected in the property derivatives [119].

effect decreases from CS<sub>2</sub> towards the heavier molecules as seen in Tables 4 and 5 of Paper VI. This arises as the magnitude of NR contribution increases steadily, whereas the effect of the SO contribution is significant only for CSe<sub>2</sub> and CTe<sub>2</sub>, being numerically almost as significant as the NR contribution in the latter. Although the first-order stretching term usually causes the main contribution, the significance of the second-order symmetric stretching motion increases towards heavier molecules at both NR and SO levels. The bending motion is responsible for the large rovibrational effect at both NR and SO levels in CTe<sub>2</sub>. Despite the fact that antisymmetric stretching motion gives a quite small contribution, this study shows that all first- and second-order contributions must be taken into account for reliable rovibrational effects, especially for heavier molecules for which the SO contribution, whose dependence of each contribution differs from the NR one, becomes very important.

In spite of the increasing temperature effect in both NR and SO contributions towards heavier X, the total temperature effect due to the rotation and vibration of the molecule is largest in CS<sub>2</sub>. This is again a consequence of cancelling contributions from NR and SO levels. The effect is particularly clear when the temperature derivatives of the <sup>13</sup>C nuclear shielding constant are compared. As the rovibrational contributions appear to be relatively insensitive to the choice of the force field, the large discrepancies between theoretical and experimental results for temperature derivatives of absolute shielding most likely originate from the solvent effects on the observed and/or reference molecule.

### *5.3.1 Isotope shifts of <sup>13</sup>C shielding constants*

The inclusion of rovibrational contributions gives an opportunity to investigate the effects of isotope substitution on the observed property. These so-called isotope effects can be classified into primary and secondary effects according to their origin: former arises from the change of the observed nucleus itself, while the latter is due to the change of isotopes of other nuclei in the system. The primary isotope shifts are experimentally very demanding as the isotope substitution changes the observed frequency range. The secondary shifts, on the other hand, are easily measured as different isotopomers give separate peaks around the main isotopomer peak in the spectrum. The peak intensities give the relative abundances of the isotopomers in the sample. Also the temperature dependence of the secondary isotope shifts is much easier to determine experimentally than in the case of the absolute shielding, where the solvent effects on both the reference and subject molecules have to be known.

As the secondary isotope shifts are experimentally more interesting, they are under investigation in Paper VI. Linear increase of the secondary <sup>13</sup>C isotope shifts with respect to the total mass of the molecule is observed both at the NR and SO levels. When the mass of the nuclei increase, the average bond lengths become shorter, causing (usually, at the NR level) larger nuclear shielding. The corresponding resonance is therefore observed at lower frequency. The SO contribution

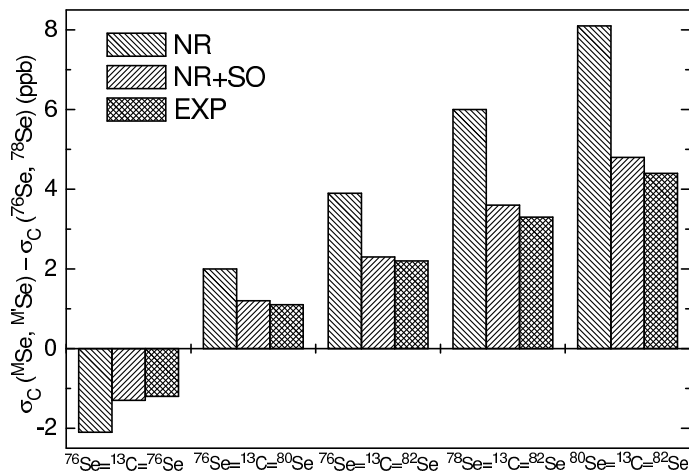


**Figure 5.1.** Comparison of the calculated and experimental secondary one-bond isotope shifts on  $^{13}\text{C}$  shielding for  $\text{CSe}_2$  at 300 K. The calculated shifts are presented both at the nonrelativistic (NR) level and with spin-orbit corrections (NR+SO).

generally decreases the positive NR isotope shift, due to the rovibrational behavior opposite to that of the NR level. Asymmetric isotope substitution, *i.e.* when the isotopes of X and X' are different, causes a relative increase of the asymmetric vibrational contribution with respect to the symmetric ones. Hence, the increasing cancellation between the opposite symmetric and asymmetric rovibrational contributions results in the decrease of the total rovibrational effect and, therefore, the asymmetric isotopomer appears to have smaller isotope shift than the symmetric isotopomer with the same mass.

The SO effects on the isotope shift are noticeable already in  $\text{CS}_2$ , where the absolute values are diminished by 5%. In  $\text{CTe}_2$ , they decrease the total shifts by half of their NR values. The most important observation is that in the case of  $\text{CSe}_2$ , the deviation of the previously calculated NR isotope shifts from the experiment [133] is totally explained by the SO effect as seen in Figure 5.1. The temperature derivatives of isotope shifts decrease due to the SO corrections, implying again a closer agreement with experiment for  $\text{CSe}_2$ , where, again, the difference by factor of two between the theoretical (NR) and experimental values [133] is explained by the SO correction. This is illustrated in Fig. 5.2 on page 57 (E-D splitting in the spectrum shown in Figure 2a of Ref. [133]). The temperature derivative of the  $^{13}\text{C}$  isotope shift in  $\text{CS}_2$  is an excellent example of the possibility of setting a goal for the experimental effort by theoretical calculations. As the experimental value appeared to be highly sensitive to the quality of the spectra, the deviation with theoretical result decreased significantly when the accuracy of the experiments was substantially improved.

SO effects on the rovibrational corrections to light atom shielding in molecules containing heavy nuclei has to be taken into account, when accurate isotope shifts as well as the temperature dependence of both the absolute shielding and isotope shifts are investigated. The previously shown examples and especially the

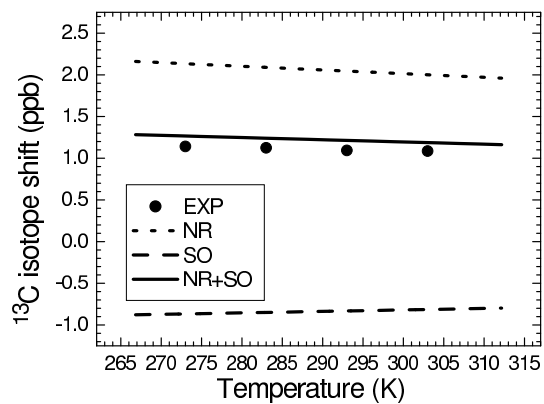


**Figure 5.2.** Calculated and experimental temperature dependence of the one-bond secondary isotope shift  $\sigma_{\text{C}}(^{80}\text{Se}, ^{80}\text{Se}) - \sigma_{\text{C}}(^{78}\text{Se}, ^{80}\text{Se})$  in  $\text{CSe}_2$ .

secondary isotope shift, clearly indicate that relativistic effects become important already for systems containing relatively light elements (already on the second row of the periodic table).

## 6 Conclusions

The present thesis provides a summary of studies concerning the computational aspects of theoretical first principles determination of magnetic (NMR) properties of molecules. While these parameters are observed experimentally by studying the response of a system of nuclear spin magnetic moments in external magnetic fields, their origin is in the complicated interactions between the nuclei and electrons in a molecule. The response of electronic states to small magnetic perturbations caused by nuclear and external magnetic fields necessitates highly accurate description of both one- and many-electron levels. In addition, the hyperfine character of NMR parameters makes them sensitive to relativistic effects. Also the vibrational and rotational motion of nuclei calls for averaging when the theoretically obtained parameters (usually obtained at the equilibrium geometry) are to be compared to experimentally observed parameters at finite temperature. Last, but not necessary the least important, factors to be taken into account, are the environmental effects due to the surrounding molecules. However, they are not covered in the present studies as they form a large area by themselves. Hence, the closest-matching real experimental condition with the calculations of the present thesis, is low density gas at finite temperature.

As currently the experimental observations of anisotropic NMR properties are carried out in liquid crystal (LC) phases, all the previously mentioned effects are present in the spectral parameters. Rovibrational corrections are also needed when theoretical values are compared with the experimental isotropic parameters observed in the gas phase. Without the treatment of rovibrational and solvent effects on either computational or experimental side, the comparison of the data can be at most qualitative.

The spin-spin coupling tensor  $\mathbf{J}$  is a very sensitive object for testing the previously mentioned theoretical concepts. Especially, the requirements for one-electron basis set are large due to the hyperfine operators, weighting the electronic structure close to or even at the nucleus, demanding highly flexible basis set expansions in the core region, typically realized with tight functions. Also, electron correlation effects are substantial, necessitating large active orbital expansions preferably with multireference character (Paper IV). Also the correlation contribution from semi-core orbitals is significant in systems containing second-row or heavier elements.

All the physical contributions should be converged at both one- and many-electron levels in order to get reliable results. When these conditions are fulfilled,  $\mathbf{J}$  tensors of quantitative accuracy at equilibrium geometry can be obtained, as seen in Papers I–IV. As the basis sets in Papers I–III are not fully converged particularly with respect to tight functions, an error of about 5% in the parameters is possible. However, both calculations and experiment of Papers I–III as well as contemporary work [77, 78] indicate that anisotropic contributions of the CF, FF, and CSi couplings,  $\frac{1}{2}J_{KL}^{\text{aniso}}$ , to experimental anisotropic dipole coupling,  $D^{\text{exp}}$ , occasionally are significant *i.e.* they should be taken into account when  $D^{\text{exp}}$  is used for the determination of structure and/or orientation of molecules in LC environment. No significant errors arise if  $\frac{1}{2}J_{KL}^{\text{aniso}}$  is neglected for CC, CH, and HH couplings.

The performance of the density-functional theory (DFT) with a hybrid functional is found in Paper V to provide  $\mathbf{J}$  of the same accuracy as the multiconfigurational self-consistent field (MCSCF) calculations of good quality, for the first- and second-row main group elements not containing many lone-pair electrons. However, as the performance of present functionals, including the hybrid ones, is dependent on the element and its surroundings, caution should be exercised in using of DFT for couplings in systems containing many lone-pair orbitals and *e.g.* transition metals. In these cases, the only justification of DFT is achieved by comparison with *ab initio* MCSCF or coupled-cluster (CC) methods. This is seldom practical for transition metal systems and, hence, DFT has to be compared to experiment rendering it a semi-empirical method.

Although in Paper VI the importance of rovibrational effects for the nuclear shielding tensor  $\sigma$  are under consideration, the same corrections [85] are necessary also for  $\mathbf{J}$  to render the theoretical result comparable with experimental coupling parameters at finite temperature. The major result of Paper VI is the remarkable relativistic spin-orbit (SO) coupling effect on the rovibrational averaging of the light atom shielding constant in systems containing heavy elements. They are qualitatively decisive for obtaining agreement with experiment for secondary isotope shifts and their temperature dependence. Even though the  $\sigma$  are somewhat less dependent on the description of correlation than  $\mathbf{J}$ , a good quality basis set is needed already at the non-relativistic level of theory. Relativistic effects, due to the high velocities of electrons near the heavy nuclei, place additional demands on the description of both one- and many-electron levels for  $\sigma$ , since contributions arising from the same operators as for the non-relativistic  $\mathbf{J}$  are present.

The density-functional linear response (DFT LR) method provides a good tool for application calculations of both NMR parameters discussed in this thesis. The method brings chemical problems related for large organic and biosystems within modeling reach. Also the new directions in the development of functionals starting from physical ideas, not fitting new semi-empirical parameters, gives hope for extending the applicability of DFT method also to systems presently out of reach. However, the strength of *ab initio* theories such as MCSCF is in their ability to produce unbiased results, when pursued far enough. Therefore, they eventually give the right answer for the right reasons, at both basis-set and correlation limits. This benchmark property makes them indispensable when new physical problems are to be solved. Of course, the current computational resources place practical

limitations for the size of the electron system. Due to the high computational cost, these methods remain practical only for quite small molecules.

The presently ongoing development in accommodating the relativistic effects and the interaction of the molecules with the surrounding solvent are two important directions in the theory of NMR parameters. These, together with the research of the present thesis constitute a complicated but fascinating and rewarding field of study.

## References

- [1] Abragam A (1961) *The Principles of Nuclear Magnetic Resonance*. Oxford University Press, Oxford.
- [2] Slichter CP (1990) *Principles of Magnetic Resonance*. Springer-Verlag, Berlin; 3<sup>rd</sup> edition.
- [3] Helgaker T, Jørgensen P & Olsen J (2000) *Molecular Electronic-Structure Theory*. John Wiley & Sons, Chichester.
- [4] Parr RG & Yang W (1989) *Density-Functional Theory of Atoms and Molecules*. Oxford University Press, Oxford.
- [5] Ramsey NF (1953) *Phys Rev* 91: 303.
- [6] Ramsey NF (1950) *Phys Rev* 78: 699.
- [7] Ramsey NF (1952) *Phys Rev* 86: 243.
- [8] Lounila J & Jokisaari J (1982) *Progr NMR Spectrosc* 15: 249.
- [9] Jokisaari J (1996) In: Grant D & Harris R (eds) *Encyclopedia of Nuclear Magnetic Resonance* John Wiley & Sons, Chichester Vol 2.
- [10] Vaara J, Jokisaari J, Wasylishen RE & Bryce DL (2002) *Progr NMR Spectrosc*, in press.
- [11] Tjandra N & Bax A (1997) *Science* 278: 1111.
- [12] Mohr PJ & Taylor BN (1999) *J Phys and Chem Ref Data* 28: 1713.
- [13] Vaara J & Pyykkö P (2001) *Phys Rev Lett* 86: 3268.
- [14] Saupe A (1964) *Z Naturforsch* 19a: 161.
- [15] Lounila J & Diehl P (1984) *J Magn Reson* 56: 254.
- [16] Lounila J & Diehl P (1984) *Mol Phys* 52: 827.
- [17] Lounila J (1986) *Mol Phys* 58: 897.
- [18] Orendt AM (1996) In: Grant DM & Harris RK (eds) *Encyclopedia of Nuclear Magnetic Resonance*. John Wiley & Sons, New York. Vol 2.

- [19] Sýkora S, Vogt J, Bösigler H & Diehl P (1979) *J Magn Reson* 36: 53.
- [20] Lounila J, Wasser R & Diehl P (1987) *Mol Phys* 62: 19.
- [21] Buckingham AD, Pyykkö P, Robert JB & Wiesenfeld L (1982) *Mol Phys* 46: 177.
- [22] Helgaker T, Jaszuński M & Ruud K (1999) *Chem Rev* 99: 293.
- [23] Buckingham AD & Malm SM (1971) *Mol Phys* 22: 1127.
- [24] Pyykkö P (1978) *Adv Quantum Chem* 11: 353.
- [25] Pyykkö P (1988) *Chem Rev* 88: 563.
- [26] Moss RE (1973) *Advanced Molecular Quantum Mechanics*. Chapman and Hall, London.
- [27] Harriman JE (1978) *Theoretical Foundations of Electron Spin Resonance*. Academic Press, New York.
- [28] Romero RH & Aucar GA (2002) *Int J Mol Sci* 3: 1.
- [29] Romero RH & Aucar GA (2002) *Phys Rev A* 65: 053411.
- [30] McWeeny R (1992) *Methods of Molecular Quantum Mechanics*. Academic Press, London: 2<sup>nd</sup> edition.
- [31] Dirac PAM (1928) *Proc Roy Soc A* 117: 610.
- [32] Dirac PAM (1928) *Proc Roy Soc A* 118: 351.
- [33] Breit G (1929) *Phys Rev* 34: 553.
- [34] Foldy LL & Wouthuysen SA (1950) *Chem Rev* 78: 29.
- [35] Aucar GA & Oddershede J (1993) *Int J Quantum Chem* 47: 425.
- [36] Ishikawa Y, Nakajima T, Hada M & Nakatsuji H (1998) *Chem Phys Lett* 283: 119.
- [37] Aucar GA, Saue T, Visscher L & Jensen HJAa (1999) *J Chem Phys* 110: 6208.
- [38] Visscher L, Enevoldsen T, Saue T, Jensen HJAa & Oddershede J (1999) *J Comput Chem* 20: 1262.
- [39] Pyykkö P (1977) *Chem Phys* 22: 289.
- [40] Pyykkö P & Wiesenfeld L (1981) *Mol Phys* 43: 557.
- [41] Fukui H, Baba T & Inomata H (1996) *J Chem Phys* 105: 3175; (1997) 106: 2987.
- [42] Schreckenbach G & Ziegler T (1997) *Int J Quantum Chem* 61: 899.
- [43] Vaara J, Ruud K, Vahtras O, Ågren H & Jokisaari J (1998) *J Chem Phys* 109: 1212.
- [44] Vaara J, Ruud K & Vahtras O (1999) *J Chem Phys* 111: 2900.
- [45] Vaara J, Ruud K & Vahtras O (1999) *J Comp Chem* 20: 1314.
- [46] Wolff SK & Ziegler T (1998) *J Chem Phys* 109: 895.
- [47] Kutzelnigg W (1999) *J Comput Chem* 20: 1199.

- [48] van Lenthe E, Baerends EJ & Snijders JG (1993) *J Chem Phys* 99: 4597.
- [49] Wolff SK, Ziegler T, van Lenthe E & Baerends J (1999) *J Chem Phys* 110: 7689.
- [50] Autschbach J & Ziegler T (2000) *J Chem Phys* 113: 936.
- [51] Autschbach J & Ziegler T (2000) *J Chem Phys* 113: 9410.
- [52] Bouten R, Baerends EJ, van Lenthe E, Visscher L, Schreckenbach G & Ziegler T (2000) *J Phys Chem A* 104: 5600.
- [53] Ballard CC, Hada M, Kaneko H & Nakatsuji H (1996) *Chem Phys Lett* 254: 170.
- [54] Hess BA (1998) In: Schleyer PvR, Allinger NL, Clark T, Gasteiger J, Kollman PA, Schaefer III HF & Schreiner PR (eds) *Encyclopedia of Computational Chemistry*. John Wiley & Sons, Chichester. Vol 2.
- [55] Fukui H & Baba T (1998) *J Chem Phys* 108: 3854.
- [56] Manninen P, Vaara J & Lantto P, in preparation.
- [57] Kutzelnigg W (1988) *Theor Chim Acta* 73: 173.
- [58] Kutzelnigg W, Ottschofski E & Franke R (1995) *J Chem Phys* 102: 1740.
- [59] Olsen J & Jørgensen P (1985) *J Chem Phys* 82: 3235.
- [60] Olsen J, Yeager DL & Jørgensen P (1989) *J Chem Phys* 91: 381.
- [61] Kirpekar S, Jensen HJAa & Oddershede J (1997) *Theor Chim Acta* 95: 35.
- [62] Kirpekar S & Sauer SPA (1999) *Theor Chem Acc* 103: 146.
- [63] Vahtras O, Ågren H, Jørgensen P, Jensen HJAa, Helgaker T & Olsen J (1993) *J Chem Phys* 97: 9178.
- [64] Lantto P, Manninen P, Vaara J & Ruud K, work in progress.
- [65] Hansen AE & Bouman TD (1985) *J Chem Phys* 82: 5035.
- [66] Kutzelnigg W (1980) *Isr J Chem* 19: 193.
- [67] Schindler M & Kutzelnigg W (1982) *J Chem Phys* 76: 1919.
- [68] London F (1937) *J Phys Radium* 8: 397.
- [69] Ditchfield R (1974) *Mol Phys* 27: 789.
- [70] Wolinski K, Hinton JF & Pulay P (1990) *J Am Chem Soc* 112: 8251.
- [71] Helgaker T & Jørgensen P (1991) *J Chem Phys* 95: 2595.
- [72] Nakatsuji H, Takashima H & Hada M (1995) *Chem Phys Lett* 233: 95.
- [73] Malkina OL, Schimmelpfennig B, Kaupp M, Hess BA, Chandra P, Wahlgren U & Malkin VG (1998) *Chem Phys Lett* 296: 93.
- [74] Hess BA, Marian CM, Wahlgren U & Gropen O (1996) *Chem Phys Lett* 251: 365.
- [75] Schimmelpfennig B (1996) *Atomic spin-orbit Mean-Field Integral program*. Stockholms Universitet.

- [76] Manninen P, Lantto P, Vaara J & Ruud K, in preparation.
- [77] Kaski J, Vaara J & Jokisaari J (1996) *J Am Chem Soc* 118: 8879.
- [78] Vaara J, Kaski J & Jokisaari J (1999) *J Phys Chem A* 103: 5675.
- [79] Vosko SJ, Wilk L & Nusair M (1980) *Can J Chem* 58: 1200.
- [80] Becke AD (1988) *Phys Rev A* 38: 3098.
- [81] Lee C, Yang W & Parr RG (1988) *Phys Rev B* 37: 785.
- [82] Becke AD (1993) *J Chem Phys* 98: 5648.
- [83] Stephens PJ, Devlin FJ, Chabalowski CF & Frisch MJ (1994) *J Phys Chem* 98: 11623.
- [84] Vaara J, Kaski J, Jokisaari J & Diehl P (1997) *J Phys Chem A* 101: 5069; (1997) 101: 9185.
- [85] Bryce DL & Wasylishen RE (2000) *J Am Chem Soc* 122: 3197.
- [86] Bryce DL & Wasylishen RE (2000) *J Am Chem Soc* 122: 11236.
- [87] Barszczewicz A, Helgaker T, Jaszunski M, Jørgensen P & Ruud K (1995) *J Magn Reson A* 114: 212.
- [88] Bartlett RJ & Purvis GD (1978) *Int J Quantum Chem* 14: 561.
- [89] Pople JA, Krishnan R, Schlegel HB & Binkley JS (1978) *Int J Quantum Chem* 14: 545.
- [90] Widmark PO, Malmqvist PÅ & Roos BO (1990) *Theor Chim Acta* 77: 291.
- [91] Widmark PO, Persson BJ & Roos BO (1991) *Theor Chim Acta* 79: 419.
- [92] Pou-Amerigo R, Merchan M, Nebot-Gil I, Widmark PO & Roos BO (1995) *Theor Chim Acta* 92: 149.
- [93] Dunning TH Jr (1989) *J Chem Phys* 90: 1007.
- [94] Woon DE & Dunning TH Jr (1993) *J Chem Phys* 98: 1358.
- [95] Helgaker T, Jaszunski M, Ruud K & Górska A (1998) *Theor Chem Acc* 99: 175.
- [96] Woon DE & Dunning TH Jr (1995) *J Chem Phys* 103: 4572.
- [97] Huzinaga S (1971) *Approximate Atomic Functions*. University of Alberta, Edmonton.
- [98] Kutzelnigg W, Fleischer U & Schindler M (1990) In: Diehl P, Fluck E, Günther H, Kosfeld R & Seelig J (eds) *NMR Basic Principles and Progress*. Springer-Verlag, Berlin. Vol 23.
- [99] Fægri K, personal communication.
- [100] Mok DKW, Neuman R & Handy NC (1996) *J Chem Phys* 100: 6225.
- [101] Møller C & Plesset MS (1934) *Phys Rev* 46: 618.
- [102] Kutzelnigg W (1985) *Theor Chim Acta* 68: 445.

- [103] Siegbahn PEM, Almlöf J, Heiberg A & Roos BO (1981) *J Chem Phys* 74: 2384.
- [104] Guilleme J & San Fabián J (1998) *J Chem Phys* 109: 8168.
- [105] Jaszuński M & Ruud K (2001) *Chem Phys Lett* 336: 473.
- [106] Sauer SPA (1997) *J Phys B* 30: 3773.
- [107] Geertsen J & Oddershede J (1986) *J Chem Phys* 85: 2112.
- [108] Geertsen J (1987) *Chem Phys Lett* 134: 400.
- [109] Sekino H & Bartlett RJ (1994) *Chem Phys Lett* 225: 486.
- [110] Perera SA, Sekino H & Bartlett RJ (1994) *J Chem Phys* 101: 2186.
- [111] Perera SA, Nooijen M & Bartlett RJ (1996) *J Chem Phys* 104: 3290.
- [112] Malkin VG, Malkina OL & Salahub DR (1994) *Chem Phys Lett* 221: 91.
- [113] Malkina OL, Salahub DR & Malkin VG (1996) *J Chem Phys* 105: 8793.
- [114] Dickson RM & Ziegler T (1996) *J Phys Chem* 100: 5286.
- [115] Sychrovsky V, Gräfenstein J & Cremer D (2000) *J Chem Phys* 113: 3530.
- [116] Helgaker T, Watson M & Handy NC (2000) *J Chem Phys* 113: 9402.
- [117] Kaski J (1999) Experimental determination of spin-spin coupling tensors applying NMR of partially oriented molecules, Ph.D. thesis, University of Oulu.
- [118] Eckart C (1935) *Phys Rev* 47: 552.
- [119] Vaara J, Lounila J, Ruud K & Helgaker T (1998) *J Chem Phys* 109: 8388.
- [120] Becke AD (2000) *J Chem Phys* 112: 4020.
- [121] Patchkovskii S, Autschbach J & Ziegler T (2001) *J Chem Phys* 115: 26.
- [122] Gauss J & Stanton JF (1995) *J Chem Phys* 102: 251.
- [123] Gauss J & Stanton JF (1996) *J Chem Phys* 104: 2574.
- [124] Ruud K, Helgaker T, Kobayashi R, Jørgensen P, Bak KL & Jensen HJAa (1994) *J Chem Phys* 100: 8178.
- [125] Schreckenbach G, Ruiz-Morales T & Ziegler T (1996) *J Chem Phys* 104: 8605.
- [126] Rauhut G, Puyear S, Wolinski K & Pulay P (1996) *J Phys Chem* 100: 6310.
- [127] Cheeseman JR, Trucks GW, Keith TA & Frisch MJ (1996) *J Chem Phys* 104: 5497.
- [128] Helgaker T, Wilson PJ, Amos RD & Handy NC (2000) *J Chem Phys* 113: 2983.
- [129] Pyykkö P, Görling A & Rösch N (1987) *Mol Phys* 61: 195.
- [130] Malkin VG, Malkina OL, Casida ME & Salahub DR (1994) *J Am Chem Soc* 116: 5898.
- [131] Toyama M, Oka T & Morino Y (1964) *J Mol Spectrosc* 13: 193.
- [132] Lounila J, Wasser R & Diehl P (1987) *Mol Phys* 62: 19.
- [133] Lounila L, Vaara J, Hiltunen Y, Pulkkinen A, Jokisaari J, Ala-Korpela M & Ruud K (1997) *J Chem Phys* 107: 1350.

## Original papers

- I Reprinted with permission from Journal of the American Chemical Society, Kaski J, Lantto P, Vaara J & Jokisaari J. Experimental and theoretical ab initio study of the  $^{13}\text{C}$ – $^{13}\text{C}$  spin-spin coupling and  $^1\text{H}$  and  $^{13}\text{C}$  shielding tensors in ethane, ethene and ethyne. 120: 3993–4005. Copyright (1998), **American Chemical Society**.
- II Reprinted with permission from The Journal of Physical Chemistry A, Kaski J, Lantto P, Schroderus J, Rantala T, Vaara J & Jokisaari J. Experimental and theoretical study of the spin-spin coupling tensors in methylsilane. 103: 9669–9677. Copyright (1999), **American Chemical Society**.
- III Reprinted with permission from Chemistry – A European Journal, Lantto P, Kaski J, Vaara J & Jokisaari J. Spin-spin coupling tensors in fluoromethanes. 6: 1395–1406. Copyright (2000), **Wiley-VCH**.
- IV Reprinted with permission from The Journal of Chemical Physics, Lantto P & Vaara J, Effect of correlating core orbitals in calculations of nuclear spin-spin couplings. 114: 5482–5490. Copyright (2001), **American Institute of Physics**.
- V Reprinted with permission from The Journal of Chemical Physics, Lantto P, Vaara J & Helgaker T, Spin-spin coupling tensors by the density-functional linear response theory. 117: 5998–6009. Copyright (2002), **American Institute of Physics**.
- VI Reprinted with permission from Journal of the American Chemical Society, Lantto P, Vaara J, Kantola A M, Telkki V-V, Schimmelpfennig B, Ruud K & Jokisaari J, Relativistic spin-orbit coupling effects on secondary isotope shifts of  $^{13}\text{C}$  nuclear shielding in  $\text{CX}_2$  ( $\text{X} = \text{O}, \text{S}, \text{Se}, \text{Te}$ ). 124: 2762–2771. Copyright (2002), **American Chemical Society**.